

ESR studies of anisotropic rotational reorientation and slow tumbling in liquid and frozen media. II. Saturation and nonsecular effects *

S. A. Goldman, G. V. Bruno[†] and J. H. Freed

Department of Chemistry, Cornell University, Ithaca, New York 14850

(Received 11 April 1973)

Careful studies are described of the ESR line shapes and saturation behavior for the peroxyamine disulfonate (PADS) radical dissolved in a range of glycerol-water mixtures. This permitted studies where the rotational correlation time τ_R ranged from 3×10^{-12} sec to $< 10^{-6}$ sec. The unsaturated line shapes for $10^{-10} < \tau_R < 10^{-9}$ sec are, as in Paper I, readily interpreted in terms of anisotropic rotational diffusion, but for $\tau_R < 10^{-10}$ sec anomalous behavior of the linewidths, which could be attributed to the nonsecular spectral densities, occurs. Supporting experiments at 35 GHz, and also on ^{17}O -labeled PADS, are in excellent agreement with values of τ_R and $N = 4.7$ (the ratio of the two components of the axially symmetric diffusion tensor), and they supply further information on the anomalous behavior of the nonsecular spectral densities. A phenomenological treatment based on the memory function approach was found to qualitatively reproduce some observed features. The saturation studies were performed over both the motional narrowing and slow-tumbling regions. The motional narrowing results could be analyzed in a straightforward manner to yield values of W_e , the electron-spin flip rate, which are found to exhibit a weak dependence on τ_R , roughly as $\tau_R^{-1/4}$ for the glycerol solvents. The stochastic Liouville method is applied to an analysis of slow-tumbling saturated spectra and generally reasonable agreement with experiment is achieved for the simplifying assumptions utilized. The rotationally invariant W_e obtained from the slow-tumbling analyses are found to agree with the values of W_e extrapolated from the motional-narrowing region. Other aspects of the slow-tumbling saturation experiments and analysis are discussed.

I. INTRODUCTION

In Paper I of this work,¹ we reported on a careful study of the ESR line shapes of the free radical peroxyamine disulfonate (PADS) in liquid and frozen media. A primary objective of that work was to compare a careful set of experiments for the slow-motional region, where $|\mathcal{H}_1(t)|\tau_R \gg 1$ [here $\mathcal{H}_1(t)$ is the rotational-dependent perturbation in the spin-Hamiltonian and τ_R is the rotational correlation time], with the theory given in Π^2 based on the stochastic Liouville method. It was indeed found that generally very good agreement could be obtained and, perhaps more interesting, that the details of reorientational motion can be reflected in the observed experimental slow-tumbling spectra. In particular, our analysis gave strong evidence for the existence of anisotropic motion and also significant deviations from a Brownian motion model. It was also shown how experiments in the motional narrowing region are very useful in supporting and clarifying the slow-tumbling work.

Another well-known source of relaxation information, hence molecular motion, is, in principle, available from saturation or T_1 data. In fact, some saturation results on the aqueous PADS system where $T_1 \cong T_2$ have previously been reported.³ However, in more viscous systems, one expects, and finds, that $T_1 > T_2$ as different relaxation mechanisms manifest themselves. In particular, the results in I show that the unsaturated line shapes are

dominated by rotational modulation of hyperfine and g tensors, while one might venture to guess that the saturation behavior continues to reflect (after significant corrections are made for the other terms) the spin-rotational relaxation mechanism postulated for the aqueous medium where $T_1 \cong T_2$.³ By slow-tumbling studies, one could effectively extend the range of temperatures and viscosities over which spin-rotational (and other electron spin-flip) mechanisms could be studied.

Two potentially important reasons for slow-tumbling saturation studies are (1) perhaps studies of saturated line shapes could also emerge as effective probes of microscopic details of molecular reorientational motion as did the study of unsaturated line shapes and (2) perhaps such techniques could be useful in extending the range over which τ_R may be measured, to slower motions than possible by unsaturated studies.^{4,5} This latter objective would be of considerable value for the study of nitroxide spin-label probes. Hyde *et al.*⁶ demonstrated that the slow-motional and polycrystalline spectra of flavin radicals have markedly different saturated line shapes, even though the unsaturated shapes were virtually superimposable. (More recent work by Hyde and Dalton⁷ has shown that the modulation frequency dependence of adiabatic rapid-passage effects may well be an effective technique to estimate very long τ_R values. An understanding of this interesting technique properly requires an understanding of saturation effects and spin relaxation in

slowly tumbling systems.)

We have, therefore, undertaken a saturation study of the PADS systems which proved to be readily amenable to careful unsaturated work. Our experiments cover the motional narrowing region, for which the saturation theory is well developed,⁸ as well as the slow-tumbling region. The basis for the theoretical analysis in the latter region is given in II for a single-line spectrum, but we have extended it for nitroxide radicals.

Our work in I also yielded an interesting preliminary result relating to that portion of the linewidths in the motional narrowing region which is due to electron-spin flip (or T_1) processes arising from dipolar and g -tensor terms, viz, the nonsecular terms. It appeared that such nonsecular terms are not simply given in terms of a Debye spectral density, but instead may be showing short-time nondiffusive properties. In the present work, we also report on our further explorations of this feature, (which, in principle, also affects saturation behavior). Besides extending the work in I, we found it useful to study ^{17}O -labeled PADS as another indicator of such effects. The inclusion of a second and different magnetic nucleus into the radical should, in principle, permit the determination of all three components of the diffusion tensor from motional narrowing experiments,⁹ and this was our initial intention since only two components are available from PADS itself. However, this work proved more useful for examining the nonsecular terms. Supporting studies at 35 GHz and the role of these nonsecular terms and anisotropic behavior on the saturation behavior are also reported.

II. EXPERIMENTAL

Most of the experimental considerations, including a description of the ESR spectrometer, given in I apply to the present work, so we only note here significant additions and changes.

The PADS was synthesized and purified by the methods described by Moser and Howie,¹⁰ yielding material which is stable indefinitely when carefully dried and stored, *in vacuo*, in a freezer. The concentration of the PADS radical in solution was determined spectrophotometrically using the maximum at 5450 Å ($\epsilon = 20.8$).¹¹ The PADS was found to have a purity of $96.7 \pm 0.5\%$. The ^{17}O -labeled PADS was synthesized and supplied to us by Luz and co-workers.^{12a} It was approximately 10% ^{17}O enriched in the nitroxide position. The aqueous PADS solutions were pH adjusted for stability with KOH at a molar concentration 5%–10% of the PADS concentration (except where explicitly noted that 0.05M K_2CO_3 buffer was used). This method of stabilization significantly reduces the electrolyte concentration,

thereby allowing the use of concentrations 2 to 3 times greater than with K_2CO_3 buffer without introducing Heisenberg exchange broadening. This results because the repulsions of pairs of PADS ions is less shielded by a reduced ionic atmosphere. Such effects have been discussed elsewhere for various amounts of buffering,^{12b} and we have extended such studies to the unbuffered solutions.^{12c}

A. Line Shape Measurements

In the motionally narrowed region with well-resolved Lorentzian lines, it is sufficient just to measure the derivative widths (δ). It is well known, however, that the relative widths are then more accurately determined from relative amplitude measurements,¹³ and this procedure was utilized. There had been a previous report of possible non-Lorentzian character for low concentration aqueous PADS solutions.¹⁴ This possibility might imply residual inhomogeneous broadening¹⁵ due to small coupling ($a/\delta < 1$) with a K^+ nucleus of $I = \frac{3}{2}$, or else perhaps field inhomogeneity. Thus ESR line shapes were carefully measured for PADS in H_2O at 21 °C, with and without K_2CO_3 buffer (Jones¹⁴ had employed the buffer) for PADS in 30% glycerol– H_2O at $T = -10$ °C, where the minimum ($\dot{M} = 0$) X-band linewidth of 92 mG is observed; and for PADS in 85% glycerol– H_2O at $T = 0$ °C. The variation of the derivative half-amplitude versus the distance from the field at resonance for the experimentally observed shapes and for Lorentzian and Gaussian line shapes is found in Table I. The half-amplitudes are normalized to unity for $(H - H_0) = \delta/2$. The experimentally observed line shapes are found to be very nearly Lorentzian with only small deviations in the wings. If an interaction with a single K^+ is assumed, then we have found a coupling constant of 15 mG would be needed to account for the small deviations from Lorentzian shapes observed in cases (1) and (3) in Table I. A comparison of the results for the buffered and nonbuffered solutions indicate that the line shape is hardly affected by the increased K^+ concentration. Magnetic field inhomogeneity could also cause these line shape deviations. It is, however, known that the field inhomogeneity is $\lesssim 5$ mG. It can be shown that these deviations from Lorentzian shape will at most broaden a 92 mG PADS line by 2%, with correspondingly smaller corrections for broader lines. Our main point then, is that the inhomogeneous broadening contributes negligible error to the relative linewidth measurements.

For the ^{17}O -labeled PADS, each ^{17}O and ^{14}N hyperfine component is inhomogeneously broadened by small couplings with ^{17}O isotope introduced, during the synthesis, into the substituent sulfate groups. For the narrower ^{14}N lines (Fig. 1), the resultant

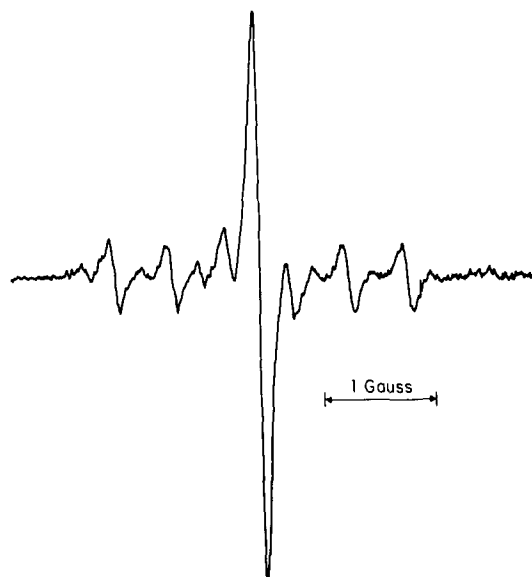


FIG. 1. ^{17}O fine structure, from labeled sulfate groups, for the $\bar{M}_N=0$ line of PADS in 30% glycerol- H_2O at -10°C .

hyperfine structure is resolved with a coupling constant of 0.54 G for a sulfate ^{17}O atom. The probability of an individual sulfate oxygen being labeled, as measured from the relative ESR amplitudes in Fig. 1, is 6.3%. With this information, it is possible to accurately simulate the non-Lorentzian nitroxide ^{17}O line shape shown in Fig. 2 and correct the observed linewidth for the effects of this inhomogeneous broadening.¹⁶ After correcting the amplitudes of the ^{17}O lines for this interaction and small overlap effects, relative linewidths could be calculated by the usual methods.

B. Saturation Technique

The technique of continuous saturation was used to determine relaxation times T_1 in the motionally narrowed region.^{3,17,18} That is, a plot of δ^2 versus

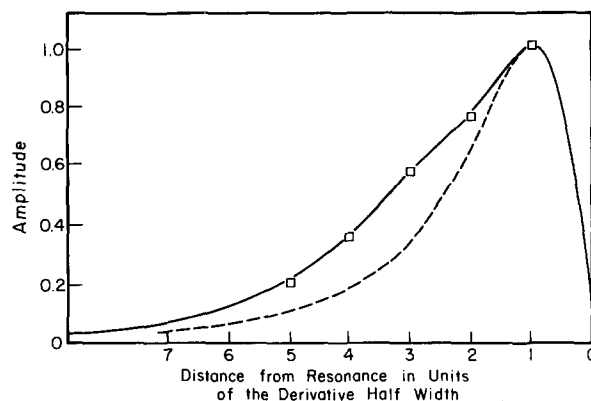


FIG. 2. Experimental and calculated line shape for the $(\bar{M}_0, \bar{M}_N) = (-\frac{5}{2}, -1)$ low field line for ^{17}O -labeled PADS in H_2O . — is the experimental line shape, --- is calculated for a Lorentzian line shape with the same derivative linewidth; (\square) is calculated for the ^{17}O coupling and intensities given in the text.

B_1^2 (microwave field squared) yields T_1/T_2 from the slope and T_2 from the intercept. The use of this relationship in the progressive saturation technique depends on the ability to accurately measure B_1^2 . As described in more detail elsewhere,^{3,17,18}

$$B_1^2 = c P_{\text{inc}} Q, \quad (2.1)$$

where P_{inc} is the incident microwave power to the cavity and Q is the unloaded cavity Q value (measured with the Dewar and sample in place but away from magnetic resonance) if, as was the case in our work, the cavity is critically coupled. The proportionality constant c is a function of the microwave field distribution and sample length. If the same Dewar is used for all experiments, c is independent of temperature and solvent variations.^{3,17,18} In our experiments, c was determined from saturation measurements on PADS in H_2O at $T=20^\circ\text{C}$. Previous experiments in this laboratory and others have shown that, for this case, $T_1/T_2=1$ within experi-

TABLE I. Comparison of PADS line shapes with a Lorentzian line shape.

| Distance from resonance in units of derivative half-width | Fraction of derivative half-amplitude ^{a,b} | | | | | | Lorentzian | Gaussian |
|---|---|---|--|--|---|-------|--------------------|----------|
| | H_2O , $T=+20^\circ\text{C}$ $\delta=0.155\text{ G}$ | $5 \times 10^{-2} M \text{ K}_2\text{CO}_3$ $T=+20^\circ\text{C}$ $\delta=0.155\text{ G}$ | 30% glycerol- H_2O $T=-10^\circ\text{C}$ $\delta=0.092\text{ G}$ | 85% glycerol- H_2O $T=0^\circ\text{C}$ $\delta=0.790\text{ G}$ | ^{17}O PADS in H_2O $T=+20^\circ\text{C}$ $\delta=1.15\text{ G}$ | | | |
| 1 | 1.0 | 1.0 | 1.0 | 1.0 | 1.0 | 1.0 | 1.0 | |
| 2 | 0.647 | 0.636 | 0.635 | 0.655 | 0.78 | 0.653 | 0.446 | |
| 3 | 0.325 | 0.323 | 0.314 | 0.332 | 0.59 | 0.353 | 0.0549 | |
| 4 | 0.171 | 0.170 | 0.165 | 0.173 | 0.36 | 0.177 | 0.0022 | |
| 5 ^a | 0.097 | 0.094 | 0.093 | 0.102 | 0.21 | 0.102 | 3×10^{-5} | |

^a Experimental uncertainty is ± 0.003 .

^b All solutions were in the exchange-free region corresponding to PADS concentrations of $1-2 \times 10^{-4} M$ except for ^{17}O PADS at $1 \times 10^{-2} M$. The solutions were $1 \times 10^{-5} M$ in KOH except for the ^{17}O PADS solution at $1 \times 10^{-3} M$ and the solution buffered with K_2CO_3 .

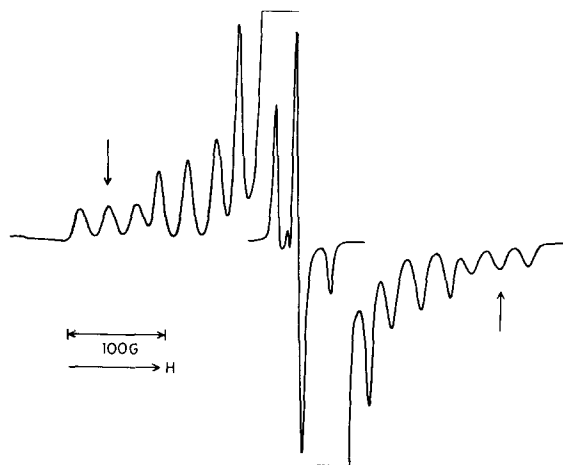


FIG. 3. X-band ESR spectrum for $2 \times 10^{-2} M$ ^{17}O -labeled PADS in 85% glycerol- H_2O at $T = -90^\circ\text{C}$. The relative gain between the ^{17}O and pure ^{14}N (central portion) lines is about 500 : 1.

mental error.^{3,17}

To insure accurate results, the cavity Q was measured for every sample and temperature for which T_1 measurements were made. Typical Q values are as follows: 7000 for a 1-mm o.d. tube of H_2O , 7120 for a 1-mm tube of 50% glycerol- H_2O , 6800 for a 2-mm tube of 85% glycerol- H_2O at $T = 20^\circ\text{C}$, and 8000 for a 2-mm tube of 85% glycerol- H_2O at $T = -90^\circ\text{C}$.

The proportionality constant in Eq. (2.1) contains a correction for the effect of the nonuniform microwave and modulating field strengths, over an ESR line sample, on the effective B_1^2 . It has been shown that for a Lorentzian line, B_1^2 (line sample)/ B_1^2 (point sample) = 0.76 for $B_1^2 T_1 T_2 \lesssim 1$.^{3,17,18} All saturation experiments in the motionally narrowed region were performed with this restriction. In the slow-motional region, however, many experiments were performed at much larger effective microwave powers. Comparisons of point vs line samples show that for the same degree of saturation, the slow-motional spectra are virtually superimposable when B_1^2 (line sample)/ B_1^2 (point sample) = 0.75 ± 0.05 . Since this is the same value found for $\gamma_e^2 B_1^2 T_1 T_2 < 1$ in the motionally narrowed region, line samples were used for subsequent slow-motional saturation experiments. No further corrections for the non-linear microwave and modulating fields were needed.

C. Rigid-Limit Simulation

The rigid-limit simulations for normal PADS are described in I. For the ^{17}O -labeled PADS, only the value of A_x could be obtained experimentally from the rigid-limit spectrum, since the lines associated with A_x and A_y parallel to the magnetic field are

buried in the rigid spectrum of the unlabeled molecule. A rigid-limit spectrum of $2 \times 10^{-2} M$ ^{17}O PADS in 85% glycerol- H_2O at $T = -90^\circ\text{C}$ is shown in Fig. 3. The relative gain between the ^{17}O and ^{14}N lines is about 500 : 1. The value of A_x (^{17}O), calculated from $\frac{1}{5}$ the separation between the peaks indicated in Fig. 3, is $A_x = 80.2 \pm 0.7$ G. Measurements on $1 \times 10^{-2} M$ ^{17}O PADS in H_2O yield a value a_N (^{17}O) = 20.91 ± 0.05 G. This value is virtually independent of solvent and temperature in the experimentally accessible region. The value of a_N in 50% glycerol- H_2O at $T = 4^\circ\text{C}$ is 20.93 ± 0.05 G. If it is assumed that the anisotropic hyperfine values are also temperature and solvent independent, then a value for $\frac{1}{2}(A_x + A_y) = \frac{1}{2}(3a_N - A_x) = -8.73$ G is obtained. Since the unpaired electron is localized in a $2p-\pi$ orbital for both ^{14}N and ^{17}O , it is reasonable to assume that the hyperfine tensors for both atoms have the same symmetry (i.e., the two $(A - a)$ tensors are nearly equal within a multiplicative constant). Comparisons with the ^{14}N data given in I indicate that a value of $A_x = A_y$ is a reasonable assumption. This was assumed for most of the subsequent analysis although the effect of small variations in A_x and A_y were also considered.

Further details on experimental procedures may be found in Goldman's thesis.¹⁶

III. RESULTS AND ANALYSIS: LINEWIDTHS

A. Further Motional Narrowing-Results (9.1 and 35 GHz)

ESR spectra for PADS in aqueous glycerol solutions were analyzed for 0, 10, 30, 50, and 85% by weight glycerol- H_2O . By varying the temperature and composition of the solvent, it is possible to vary τ_R continuously from 3.5×10^{-12} sec, for PADS in H_2O at $T = 23^\circ\text{C}$, to the rigid limit for the 85% glycerol- H_2O solvent at $T \lesssim -90^\circ\text{C}$. The accessible temperature range for each solvent was determined by the freezing point of the mixture and the temperature at which PADS began to decompose. The possibility of obtaining $\tau_R \gtrsim 3.5 \times 10^{-12}$ sec permitted a more careful analysis of deviations of nonsecular contributions from those expected for a Debye spectral density (cf. Sec. I).

The experimental results are analyzed in the usual way in terms of the expression $\delta = A + B\bar{M}_N + C\bar{M}_N^2$, where \bar{M}_N is the ^{14}N spectral-index number.¹³ The complete results for the variation of B vs C for the entire range of glycerol- H_2O mixtures are given in Fig. 4. In the regions where the linewidth results for different compositions overlap, the values of B vs C are the same within experimental error. The results for A are given in Fig. 5. The uncertainty in A is found to be $\sim 1\%$, while that for B and C is 1%–3% for the 85% and 50% glycerol- H_2O solutions. When the value of B and C becomes small compared

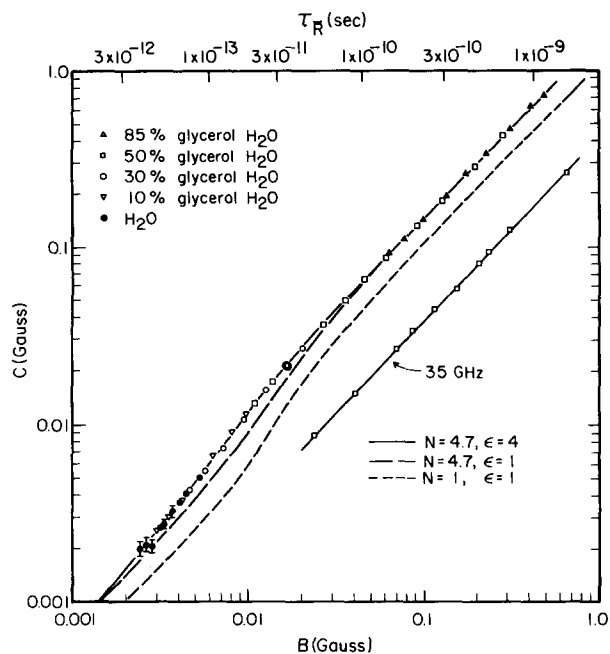


FIG. 4. A comparison of experimental and calculated values of B vs C for PADS in glycerol-H₂O. The τ_R shown are for the X-band results. For 35 GHz, the correct τ_R values are those corresponding to the X-band experimental results with the same value for C as the 35 GHz results.

to A , i.e., B/A , $C/A < 0.05$, the uncertainty in B and C increases to about 3%–5%.

The results in Fig. 4 for $\tau_R > 10^{-10}$ sec (as was found in I for just PADS in 85% glycerol-H₂O) may be fit very well by an axially symmetric rotational diffusion model, where $N = R_3/R_1 = 4.7 \pm 1$. Here $\tau_R = (6\bar{R})^{-1}$ and $\bar{R} = (R_3R_1)^{1/2}$ [and the predicted linewidths are based on Eq. (5) of I]. However, we note that for $\tau_R \sim \omega_0^{-1} = 1.75 \times 10^{-11}$ sec, the experimental results deviate from the predictions. (This is consistent with the earlier study of PADS in ice which, however, only ranged from $\tau_R > 10^{-11}$ sec.) However, for $\omega_0^2 \tau_R^2 \ll 1$, i.e., $\tau_R \lesssim 4 \times 10^{-12}$ sec, the experimental results and the predicted values for $N = 4.7$ again appear to converge within experimental error.

In I we have presented strong arguments (and results) against any significant changes in the magnetic parameters, which could otherwise lead to such discrepancies. It was also argued that it is not likely for N , which again appears to be constant from $\tau_R = 10^{-9}$ sec to 10^{-10} sec, to begin to change appreciably and nonmonotonically for $\tau_R < 10^{-10}$ sec. However, it was possible to obtain additional evidence from 35 GHz studies against a temperature dependence of the spin parameters and/or the anisotropy of the rotational diffusion which could af-

fect linewidths.

At 35 GHz, $\omega_0^{-1} = 4.6 \times 10^{-12}$, and nonsecular terms are negligible for $\tau_R \gtrsim 3 \times 10^{-11}$ sec. Thus if there were any experimental variation in C/B at 35 GHz for $\tau_R > 3 \times 10^{-11}$, it must be caused by changes in magnetic parameters or N . The 35 GHz results where τ_R ranges from 1.4×10^{-11} sec to 4×10^{-10} sec, given in Fig. 4, indicate that within experimental error, C/B is independent of τ_R and temperature for $\tau_R > 3 \times 10^{-11}$ sec. [The values of τ_R and N are obtained from Eq. (5) of I.] The calculated values of $N = 4.5 \pm 1$ are consistent with the X-band results of $N = 4.7 \pm 1$ for longer τ_R . If the values of C/B are scaled to 9.1 GHz, the resultant values of 1.48 ± 0.08 are just what would be expected from Fig. 4 and Eq. (5) of I for $N \sim 4.7$ in the absence of nonsecular terms.

These results, coupled with the fact that the X-band results for the H₂O solvent are also consistent with $N = 4.7$, strongly imply that within the accuracy of the linewidth measurements, the magnetic parameters and N are solvent and temperature independent over the whole range of glycerol-H₂O compositions. The 35 GHz and X-band results, for $\tau_R \sim \omega_0^{-1}$, would be in disagreement if both sets of linewidth data are interpreted with nonsecular terms treated in the standard way. The value of N calculated from Eq. (5) of I for $\tau_R \cong 3 \times 10^{-11}$ sec is 4.0 ± 1 and 8.2 ± 1 at 35 GHz and X-band, respectively. For the former, nonsecular terms are almost negligible, and the calculated value of N agrees with the X-band results obtained for $\omega_0^2 \tau_R^2 \gg 1$. For the latter calculated result, nonsecular terms, treated in the standard way, make a significant contribution to the linewidth.

The dashed line in Fig. 4 was calculated from Eq. (5) of I based on the approximation of axially symmetric instead of totally asymmetric rotational

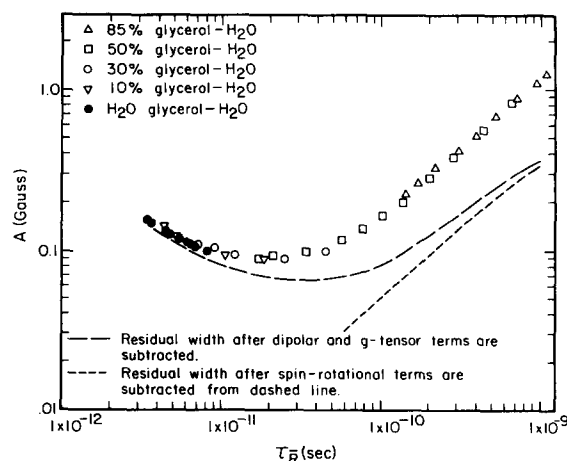


FIG. 5. A vs τ_R for PADS in glycerol-H₂O solutions.

diffusion. In order to ascertain whether this approximation affects the calculated C/B ratios for $\tau_R \sim \omega_0^{-1}$, Eq. (5) of I was modified for totally asymmetric rotational diffusion as described in detail by Freed.^{9,19} Calculations performed for an asymmetric diffusion model, in the region where nonsecular terms are important, show some variation in the calculated C/B ratio as R_x and R_y are varied from the value of R_1 . For $\omega_0^2 \tau_R^2 \gg 1$ only two diffusion parameters, R_{11} and R_{12} , are needed to fit the experimental data. The results for axial diffusion, given in I demonstrate that the experimental results for $\omega_0^2 \tau_R^2 \gg 1$ could only be fit with $R_y > R_x$, R_z . Thus initial values of R_y/R_x and R_y/R_z greater than 1 were chosen and the third diffusion constant was adjusted to fit the results for $\omega_0^2 \tau_R^2 \gg 1$ and $R_{11}/R_{12} = 4.7$. Keeping the relative values of R_i constant, the absolute values were then varied until the value for C calculated for $\tau_R = 3 \times 10^{-11}$ sec and $R_{11}/R_{12} = 4.7$ was obtained. For these values of R_i , the C/B ratio was calculated and compared to the results for axial diffusion and $N = 4.7$. Results were obtained for ratios of R_y/R_x and R_y/R_z of 10 and 100. (Although these values are unrealistically large, it was felt that they would encompass all possible calculated variations of the C/B ratio.) The calculated C/B ratio was found to vary only a few percent from the value calculated for axial diffusion. The variation among these values (1.10–1.13) is small compared to the difference between the calculated results and the experimentally observed C/B ratio of 1.30 ± 0.06 . Thus the approximation of axial versus completely asymmetric diffusion cannot account for the differences between the experimental points and the dashed line, calculated for $N = 4.7$, in Fig. 4. These results indicate that in the region where nonsecular terms are important (and where the condition that $\omega_0^2 \tau_R^2 \ll 1$ is still not true), the usual spin-relaxation expressions for these terms do not properly represent their contribution to the linewidth.

As discussed in I, the dependence of the nonsecular spectral density on τ_R is given by the Fourier transform of the correlation function $g(\tau)$

$$\equiv \langle \mathcal{D}_{KM}^L *(\tau) \mathcal{D}_{KM}^L(0) \rangle$$

$$j(\omega_0, \tau_R) = \frac{1}{2} \int_{-\infty}^{\infty} g(\tau) e^{-i\omega_0 \tau} d\tau \quad (3.1)$$

The standard Debye-type result of

$$j(\omega_0, \tau_R) = \tau_R / (1 + \omega_0^2 \tau_R^2) \quad (3.2)$$

is obtained with the usual assumption of an exponential decay of the correlation [$g(\tau) \propto e^{-\tau/\tau_R}$].

We have found it convenient to fit the linewidth results for glycerol–H₂O in a purely empirical fashion with

$$j(\omega_0, \tau_R) = \tau_R (1 + \epsilon \omega_0^2 \tau_R^2)^{-1}, \quad (3.3)$$

where ϵ is an adjustable parameter not to be con-

fused as a modification of τ_R . (Such a parameter may be related to the more fundamental memory function approach as discussed in Sec. III.C). The best fit is obtained with $\epsilon = 4$. It can be seen in Fig. 4 that the solid line, drawn for this value of ϵ , is consistent with the experimental results. The values of τ_R obtained from this functional form are within 5% of those calculated using the usual expression for the nonsecular terms. However, for the entire range of glycerol–H₂O compositions, the results fall in the range of $N = 4.7 \pm 1$,²⁰ when $\epsilon = 4$ is utilized.

The variation of A with τ_R is shown in Fig. 5. The contribution of the dipolar and g -tensor terms to this linewidth can be calculated from the experimental values of τ_R and N using Eq. (5) of I. The dashed line in Fig. 5 is the residual width X after these contributions are subtracted. For $\tau_R \lesssim 3 \times 10^{-11}$ sec, the increase in this residual width can be attributed to the increased contribution of spin-rotation to the linewidth. The increase in X for $\tau_R > 3 \times 10^{-11}$ sec is similar to the results observed for PADS in frozen H₂O.¹

A comparison of the X-band and 35 GHz $\tilde{M} = 0$ linewidth results shows that this residual width is magnetic-field independent. For PADS in 50% glycerol H₂O at $T = -30^\circ\text{C}$ ($\tau_R = 4.05 \times 10^{-10}$ sec) the 35 GHz $\tilde{M} = 0$ linewidth is 923 ± 50 mG after exchange contributions are subtracted. The dipolar and g -tensor contribution to this width, calculated from Eq. (5) of I, is 687 ± 30 mG, which leaves a residual width of 236 ± 80 mG. The residual width for this τ_R value at X band is 210 ± 15 mG. Thus, the X-band and 35 GHz residual widths are the same within experimental error. (We estimate ~ 15 mG extra inhomogeneous broadening of the 35 GHz line over the X-band line by comparison of X-band and 35 GHz. $\tilde{M} = 0$ widths at 19°C for a 10^{-3} M sample of PADS in H₂O. Here $\tau_R \approx 3.5 \times 10^{-12}$ sec and the respective widths are 169 and 148 mG with an estimated extra g -tensor contribution to the 35 GHz width of ~ 7 mG.)

We have made the reasonable assumption that X for $\tau_R < 8 \times 10^{-12}$ sec is due mainly to a spin-rotational interaction based on the results of Kooser *et al.*³ showing $T_1 \approx T_2$ for PADS in H₂O. The dotted line in Fig. 5 shows the remaining residual width after the estimated spin-rotational relaxation contribution [which fulfills the relation $(T_2^{-1})^{\text{SR}} = 2W_{\text{SR}}^{\text{SR}}(0)$, cf. Sec. IV] is subtracted. This residual width is found to increase almost linearly with τ_R . The possibility that intermolecular electron spin-spin interactions are the source of this may be discarded since the results of Fig. 5 are found to be independent of the PADS concentration for concentrations less than 5×10^{-4} M. It is possible to analyze this

residual width in terms of electron-spin-solvent-proton dipolar interactions to obtain results for the translational diffusion coefficient D that are reasonable for glycerol solvents,¹⁶ but recent results on other systems utilizing perdeuterated solvents suggest that only part of this residual width may be assigned to this interaction.²¹ Related matters are discussed in Sec. IV.

B. Linewidth Study of ¹⁷O PADS

Linewidth results for 10⁻² M ¹⁷O-labeled PADS in H₂O were obtained for $T=21, 13,$ and 5°C . At higher temperatures the PADS began to decompose, and for $T < 5^\circ\text{C}$, or more viscous solutions, the overlap of the ¹⁷O lines makes accurate linewidth analysis impossible. Even though the high PADS concentration used for these solutions resulted in some exchange broadening, it was necessary for an adequate signal-to-noise ratio. Of the 18 lines observed for the $I = \frac{5}{2}$ ¹⁷O and $I = 1^{14}\text{N}$ nuclei, only 10 lines were sufficiently resolved for accurate linewidth measurements. The interior 8 lines were overlapped with the much more intense spectrum of the unlabeled PADS molecules. The relative linewidths were measured from the relative amplitudes as described in Sec. II. The absolute linewidth of the ($\tilde{M}_0 = -\frac{5}{2}; \tilde{M}_N = -1$) low field line was measured with an uncertainty of 1%–2%.

The linewidth data can be fit to the expression^{12,13}

$$\delta = A + B_N \tilde{M}_N + B_0 \tilde{M}_0 + C_N \tilde{M}_N^2 + C_0 \tilde{M}_0^2 + D \tilde{M}_N \tilde{M}_0, \quad (3.4)$$

where \tilde{M}_0 and \tilde{M}_N are the spectral index numbers for ¹⁷O and ¹⁴N, respectively. For $T=13$ and 21°C , A is given as $A = A_N + A_0$, where A_N is the $\tilde{M}_N = 0$ linewidth for the unlabeled nitroxide. A_0 , which is the difference between A and A_N , is the additional $\tilde{M}_N = \tilde{M}_0 = 0$ width due solely to the presence of the ¹⁷O magnetic nucleus. The linewidth contributions from exchange, spin-rotation and pure g -tensor terms are all included in A_N . Since $B_N/B_0, C_N/C_0 \ll 1$, the values of B_N and C_N at these temperatures may be taken from the ¹⁴N data in Fig. 4. The contribution from these terms was then subtracted from the linewidths for the ¹⁷O-PADS. The resultant linewidths were least-squares fit to

$$\delta = A + B_0 \tilde{M}_0 + C_0 \tilde{M}_0^2 + D \tilde{M}_0 \tilde{M}_N. \quad (3.5)$$

The values of $A, A_0, B_0, C_0,$ and D , and their standard deviations are given in Table II.

An expression for T_2^{-1} (¹⁷O), the extra linewidth terms resulting from the presence of the $I = \frac{5}{2}$ oxygen, is obtained in a manner analogous to Eq. (5) of I. The linear and quadratic terms in M_0 are the same as those given in Eq. (5) of I except that the ¹⁷O dipolar tensor components are now used. The ¹⁷O \tilde{M}_0 independent terms are identical to the \tilde{M}_N independent dipolar terms in Eq. (5) of I. An ex-

TABLE II. Least-squares analysis for ¹⁷O PADS linewidth results.

| | $T=21^\circ\text{C}^a$ | $T=13^\circ\text{C}^a$ | $T=5^\circ\text{C}^a$ |
|-----------|------------------------|------------------------|-----------------------|
| A^b | 0.801 ± 0.003 | 0.869 ± 0.002 | 0.986 ± 0.004 |
| A_0^c | 0.571 ± 0.017 | 0.668 ± 0.016 | ... |
| B_0^b | 0.0099 ± 0.0005 | 0.0125 ± 0.0003 | 0.0147 ± 0.0007 |
| C_0^b | 0.0261 ± 0.0005 | 0.0319 ± 0.0003 | 0.0398 ± 0.0007 |
| D_0^b | 0.0462 ± 0.0006 | 0.0543 ± 0.0004 | 0.0660 ± 0.0009 |
| C_0/B_0 | 2.64 ± 0.17 | 2.54 ± 0.08 | 2.70 ± 0.15 |
| A_0/C_0 | 21.9 ± 1.0 | 21.0 ± 0.7 | ... |

^aUnits are in gauss.

^bThe error statistics are only for the relative values of $A, B_0, C_0,$ and D . There is an additional uncertainty of $\sim 1.5\%$ in all the values.

^cThe error statistics represent the total uncertainty in A_0 .

pression for the $M_N M_0$ cross terms is^{9,22}

$$T_2^{-1}(M_N M_0) = (4\pi^2/5) \xi^2 (D_N^{(0)} D_0^{(0)}) \tau(0) \times \{ (16/3) + 4[1 + \omega_0^2 \tau(0)^2]^{-1} \} + 2D_N^{(2)} D_0^{(2)} \tau(2) \times \{ (16/3) + 4[1 + \omega_0^2 \tau(2)^2]^{-1} \} \quad (3.6)$$

when it is assumed that the nitrogen and oxygen hyperfine tensors are colinear (cf. Sec. II.C). It is seen from Eqs. (3.4) and (3.5) that the ¹⁷O PADS introduces four new independent experimental parameters from which to obtain further information on the rotational diffusion (e.g., all three components $R_x, R_y,$ and R_z of the diffusion tensor). However, the collinearity of the two hyperfine tensors means that they cannot supply different information on the diffusion tensor, but they can serve to confirm the results on N already obtained with unlabeled PADS, and furthermore, the new types of terms A_0 and D can be used for independent information on our ad hoc experimental parameter ϵ .

A number of factors have to be considered in analyzing the results in Table II with Eqs. (5) of I and (3.6). The experimental results are obtained in a motional region where nonsecular terms are important but the condition that $\omega_0^2 \tau_{2,m}^2 \ll 1$ is not quite fulfilled. An analysis of Eq. (5) of I shows that in the extreme narrowing limit for $\omega_0^2 \tau_{2,m}^2 \ll 1$ or $j(\omega_0, \tau_{2,m}) = \tau_{2,m}, A_0/C_0 = (\frac{5}{3})I(I+1) = 21.88$ for $I = \frac{5}{2}$. This result is independent of the values of the ¹⁷O hyperfine tensor components. Since nonsecular terms contribute more to A_0 than to C_0 , the value of A_0/C_0 decreases as the relative nonsecular contribution to the linewidths decreases for longer τ_R [For $\omega_0^2 \tau_R^2 \gg 1, A_0/C_0 = (\frac{3}{5})I(I+1) = 5.25$.] The results in Table II, for $T=22^\circ\text{C}$, show that the experimental value for A_0/C_0 is exactly what would be predicted for $\omega_0^2 \tau_{2,m}^2 \ll 1$ or $\epsilon = 0$ in Eq. (3.3). The value of A_0/C_0 for $T=13^\circ\text{C}$ is only slightly lower

than this theoretical limit. A smaller value of A_0/C_0 at this τ_R is calculated for $\epsilon=4$, which fits the ^{14}N linewidth data, and for $\epsilon=1$ which is derived for Brownian diffusion. Thus it is important to evaluate how the choice of $j(\omega_0, \tau_R)$ affects the ^{17}O linewidth analysis. The nonsecular terms were introduced with Eq. (3.3) for $\epsilon=1$ and 4. For the purpose of comparison, a value of $\epsilon=0$, which is equivalent to the extreme narrowing limit, was also used.

The preliminary analysis of the ^{17}O linewidth results was performed assuming $A_x=A_y=(3a_N-A_x)/2$. This assumption is reasonable based on the ^{14}N rigid limit results of Sec. II. C. It is important, however, to estimate the effects of small variations in the values of A_x and A_y on the analysis. Thus, calculations were also performed for $A_x-A_y=\pm 6$ G with $(A_x+A_y)/2$ kept constant. The effect of the uncertainty in $A_x(^{17}\text{O})$, the g -tensor components, and the ^{14}N hyperfine tensor components was also considered.

The following procedure was used in fitting the experimental data in Table II: (1) For a given value of A_x-A_y and ϵ , τ_R and N were determined from the experimental values of C_0 and B_0 using the theoretical expression for ^{17}O linewidths which is analogous to that given in Eq. (5) of I for ^{14}N (as noted above); this supplies two equations for the two unknowns. (2) These values were then used to calculate D and A_0/C_0 . (3) The uncertainty in these latter quantities was determined by varying τ_R and N over the range of values consistent with the experimental error of C_0 and B_0 . These results, summarized in Table III, are the values calculated for $A_x=A_y$ and $\epsilon=0, 1, \text{ and } 4$. The first set of error limits is the uncertainty in these quantities as described above. The second set of error limits reflect the variation in these quantities for $A_x-A_y=\pm 6$ G relative to the values calculated for $A_x=A_y$. Except for A_0/C_0 , the minus signs correspond to

$A_x-A_y=+6$ G. The reverse is true for $A_x+A_y=-6$ G. The uncertainty in $A_x(^{17}\text{O})$ and the g -tensor components correspond to an additional uncertainty of ± 0.7 in N . This coupled with the error in the ^{14}N hyperfine values results in an additional uncertainty of 5%, 2%, and 1.5% in the value of D for $\epsilon=0, 1, \text{ and } 4$, respectively. The value of A_0/C_0 is not affected by these additional considerations.

An analysis of the results in Table III and a comparison with the experimental data in Table II yields the following observations. The calculated value of τ_R is only slightly sensitive to the choice of ϵ . Thus τ_R changes by only $\pm 1\%$ - 2% as ϵ varies from 0 to 4. The variation in the value of A_x-A_y results in an additional 5% change in τ_R . These results are in excellent agreement with the τ_R values obtained for ^{14}N PADS in Fig. 4 for aqueous solvent at the same temperatures and provide an independent verification of the accuracy of the τ_R values.

A comparison of the experimental and calculated values of A_0/C_0 for $T=13$ and 22°C indicates that they cannot be fit with $\epsilon=4$. The disagreement between the experimental results and the values calculated for $\epsilon=4$ is larger than any possible errors in the calculated numbers. This implies that the $j(\omega_0, \tau_R)$, which fit the ^{14}N data for $\tau_R > \omega_0^{-1}$, is not applicable for $\tau_R < \omega_0^{-1}$ or $\tau_R \sim 4 \times 10^{-12}$ sec. The results for $\epsilon=0$ and 1 are more ambiguous. For $T=22^\circ\text{C}$, good agreement is obtained for $\epsilon=0$, while the calculated value of A_0/C_0 for $\epsilon=1$ is slightly small. For $T=13^\circ\text{C}$ the experimental result is midway between those calculated for $\epsilon=0$ and 1.

A comparison of the calculated and experimental values of D confirms the fact that the results cannot be fit with $\epsilon=4$. The best agreement is obtained for $\epsilon=1$ and $A_x=A_y$. These values agree almost perfectly with the experimental results at $T=22, 13, \text{ and } 5^\circ\text{C}$. The values calculated with $\epsilon=0$ are in general larger than the experimental results.

TABLE III. Linewidth analysis for ^{17}O PADS.

| $T(^{\circ}\text{C})$ | ϵ^a | $\tau_R \times 10^{12}$ (sec) ^b | N^b | D_0 (mG) ^b | A_0/C_0^b |
|-----------------------|--------------|--|------------------------|-------------------------|-------------------------|
| + 21 | 0 | $3.59 \pm 0.07(\pm 0.27)$ | $5.5 \pm 1(\pm 2)$ | $48.9 \pm 2.5(\pm 4.5)$ | 21.88 |
| | 1 | $3.53 \pm 0.07(\pm 0.27)$ | $4.8 \pm 1(\pm 2)$ | $45.7 \pm 1.8(\pm 2.8)$ | $20.0 \pm 0.4(\pm 0.8)$ |
| | 4 | $3.48 \pm 0.07(\pm 0.27)$ | $3.8 \pm 1(\pm 1.8)$ | $41.8 \pm 1.4(\pm 1.7)$ | $17.6 \pm 0.4(\pm 1.0)$ |
| + 13 | 0 | $4.40 \pm 0.04(\pm 0.24)$ | $4.9 \pm 0.4(\pm 1.6)$ | $59.5 \pm 1.3(\pm 3.4)$ | 21.88 |
| | 1 | $4.35 \pm 0.04(\pm 0.24)$ | $4.0 \pm 0.4(\pm 1.6)$ | $55.0 \pm 0.9(\pm 1.9)$ | $19.6 \pm 0.3(\pm 0.6)$ |
| | 4 | $4.26 \pm 0.04(\pm 0.24)$ | $3.0 \pm 0.4(\pm 1.2)$ | $50.0 \pm 1.0(\pm 1.3)$ | $17.1 \pm 0.3(\pm 0.7)$ |
| + 5 | 0 | $5.38 \pm 0.09(\pm 0.39)$ | $6.0 \pm 1(\pm 2.5)$ | $74.5 \pm 2.7(\pm 6.7)$ | ... |
| | 1 | $5.32 \pm 0.09(\pm 0.39)$ | $4.5 \pm 0.8(\pm 1.8)$ | $66.1 \pm 2.1(\pm 3.0)$ | ... |
| | 4 | $5.22 \pm 0.09(\pm 0.29)$ | $3.2 \pm 0.7(\pm 1.5)$ | $59.0 \pm 2.2(\pm 2.4)$ | ... |

$$^a j(\omega_0, \tau_R) = \tau_R (1 + \epsilon \omega_0^2 \tau_R^2)^{-1}$$

^bThese values are calculated for $A_x=A_y$ for the ^{17}O hyperfine tensor. The error limits in parenthesis are based on the range of possible values for $A_x-A_y=\pm 6$ G.

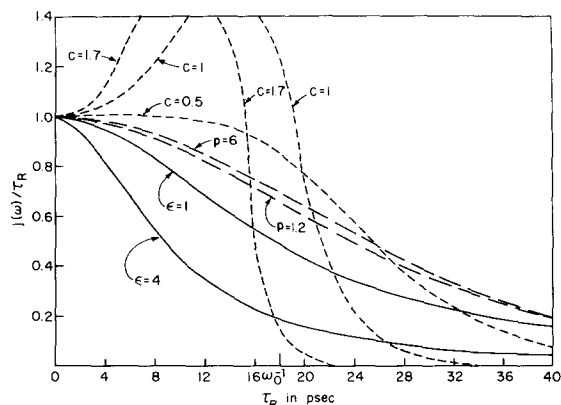


FIG. 6. Comparison of spectral densities $j(\omega_0)$ as a function of $\tau_R \equiv j(0)$ for different functional forms with $\omega_0^{-1} = 1.7 \times 10^{-11}$ sec. The solid curves are from Eq. (3.3); the broken line curves are from Eq. (3.8); the dashed lines are from Eq. (3.13) with $c \equiv \tau_G/\tau_R$. For the cases of $c=1$ and 1.7 maxima (not shown) occur at coordinates $[j(\omega)/\tau_R; \tau_R]$ of (1.66, 14.2) and (3.25, 10.4), respectively.

(However, for $A_x - A_y = 6$ G, when the deviations in the spin parameters are considered, the experimental values can be obtained for $\epsilon = 0$. The ^{14}N results, however, show that $\epsilon = 0$ is unrealistic for longer τ_R .)

The value of N calculated for $\epsilon = 1$ and $A_x = A_y$ fall in the range of $N = 4.4 \pm 0.4$. If the $\epsilon = 0$ results are considered then $N = 5.5 \pm 0.6$. These results are consistent with the $N = 4.7 \pm 1$ found for N^{14} PADS and $\omega_0^2 \tau_R^2 \gg 1$.

In summary, the ^{17}O linewidth results confirm the values of $\tau_{\bar{R}}$ and N found for ^{14}N PADS in the glycerol- H_2O systems. If the contribution of the nonsecular terms to the linewidth, in this region, is to be described by Eq. (3.3), then a value of $\epsilon \approx 1$ is needed to fit the value of D and A_0/C_0 simultaneously.

These results indicate that the usual expression for the nonsecular terms, with $\epsilon = 1$, is adequate for $\tau_{\bar{R}} \leq 5 \times 10^{-12}$ sec, while the ^{14}N results for $\tau_{\bar{R}} \gtrsim \omega_0^{-1}$ are best fit with Eq. (3.3) and $\epsilon = 4$.

C. Further Comments

We have made a simple attempt to attach some physical significance to the experimental adjustment parameter ϵ which is ~ 4 for $\tau_{\bar{R}} \gtrsim \omega_0^{-1} = 1.7 \times 10^{-11}$ sec and ~ 1 for $\tau_{\bar{R}} \lesssim 5 \times 10^{-12}$ sec. We have utilized the nonexponential correlation function

$$g(\tau) = \exp\{-6R\tau[\exp(-t/\tau) - 1 + t/\tau]\} \quad (3.7)$$

as suggested in I for a simple model which includes "short-time" inertial effects. In this interpretation one may take $\tau = I/\xi$, where I is the moment of in-

ertia and ξ the rotational friction coefficient with $R = kT/\xi$. We then obtain²³

$$j(\omega) = \tau e^{\beta} \text{Re}[p^{-\alpha} \gamma(z, \beta)], \quad (3.8)$$

where $\beta = 6R\tau$, $z = \beta + i\omega$, and $\gamma(z, \beta)$ is the incomplete gamma function. Note that

$$\tau_R \equiv j(0). \quad (3.8')$$

We compare in Fig. 6, the values of $j(\omega_0)$ as given by Eq. (3.8) for several large values of β with those of Eq. (3.3) for $\epsilon = 1$ and 4. It is clear that there is no reasonable relation between the two types of expressions. (The $\beta = 1.2$ and 6 curves do ultimately cross the $\epsilon = 4$ curve, but at $\tau_R = 10^{-10}$ and 7×10^{-11} sec, respectively.)

As an alternative approach to analyzing the $\epsilon \neq 1$ results in terms of deviations from Debye-type spectral densities, we have utilized the memory function approach in a simple phenomenological manner.²⁴ That is, one can write^{24,25}

$$dg(t)/dt = - \int_0^t \tilde{\gamma}(t')g(t-t')dt' \quad (3.9)$$

so from Eq. (3.1) one has

$$j(\omega) = \gamma'(\omega) / \{[\omega + \gamma''(\omega)]^2 + [\gamma'(\omega)]^2\}, \quad (3.10)$$

where

$$\gamma(\omega) \equiv \gamma'(\omega) + i\gamma''(\omega) \equiv \int_0^\infty \tilde{\gamma}(t)e^{-i\omega t} dt \quad (3.10')$$

with $\gamma'(\omega)$ and $\gamma''(\omega)$ real quantities which are, respectively, even and odd functions of ω . Again τ_R is defined by Eq. (3.8'), so $\tau_R = \gamma'(0)^{-1}$. [One may note that if $\gamma'(\omega)$ and $\gamma''(\omega)$ are expanded in power series in ω , and only lowest order terms are kept, then we would have $\gamma'(\omega) \approx \tau_R^{-1}$ and $\gamma''(\omega) \approx \alpha\omega$, where α is a constant properly determined from molecular dynamics. If these approximations are substituted into Eq. (3.10), then a comparison of the resulting expression with Eq. (3.3) yields a simple expression for the empirical parameter ϵ as $\epsilon \approx (1 + \alpha)^2$. The models discussed below, however, suggest that for substantial deviation of ϵ from unity, such a lowest order expansion is not an adequate expression for ϵ , and, although a formal and complex expression may be obtained for ϵ by equating Eqs. (3.3) and (3.10), it is best regarded in a purely empirical sense. The kernel $\tilde{\gamma}(t')$ has the property of a memory function, and it, in principle, contains the information about the coupling of the reorientation of the radical probe to all the other relevant degrees of freedom. [In this sense, the free-diffusion model of Eq. (3.7) could be reformulated as a memory function.] Rather than attempting a complete analysis of $\tilde{\gamma}(t)$ at this time from the microscopics of different models we assume simple functional forms for $\tilde{\gamma}(t)$,²⁴ i. e.,

$$\gamma'_s(\omega) = \gamma_s / [1 + (\omega\tau_s)^2], \quad (3.11a)$$

$$\gamma_s''(\omega) = -\omega\tau_s\gamma_s'(\omega), \quad (3.11b)$$

corresponding to an exponential memory function

$$\tilde{\gamma}_s(t) = (\gamma_s/\tau_s)e^{-t/\tau_s} \quad (3.12)$$

or

$$\gamma_G(\omega) = \gamma_G w(-\omega\tau_G), \quad (3.13)$$

where

$$w(x) \equiv e^{-x^2} \operatorname{erfc}(-ix) \quad (3.13')$$

and $\operatorname{erfc}(x)$ is the complementary error function, corresponding to a Gaussian memory function

$$\tilde{\gamma}_G(t) = (\gamma_G/\tau_G\sqrt{\pi})e^{-t^2/4\tau_G^2}. \quad (3.14)$$

{Note that as τ_s (or τ_G) approaches zero $\tilde{\gamma}_s(t)$ [or $\tilde{\gamma}_G(t)$] become delta functions so that from Eq. (3.9), $g(t)$ gives simple exponential decay with $\gamma_s(0)^{-1} = \tau_R$, etc.; while as τ_s (or τ_G) becomes very long, dynamical coherence persists, and a more rigorous analysis may be called for.}

We show in Fig. 6 curves plotted for the Gaussian memory function for several values of $c \equiv \tau_G/\tau_R$. We note that for a $c = 1.7$ one has at $\tau_R \approx \omega_0^{-1}$ the equivalent of an $\epsilon \approx 5$, but the effective ϵ value is rapidly changing, and at $\tau_R \sim 10^{-11}$ sec, $j(\omega)/\tau_R$ in fact shows a strong maximum. For $c = 0.5$, however the behavior for $\tau_R < 10^{-11}$ is more satisfactory, corresponding to an $\epsilon \approx 0$, but for $\tau_R > 10^{-11}$ sec it is not decreasing soon enough. We wish, however, to note the following two points: (1) c itself can be expected to be a function of temperature and (2) the Gaussian form, although a common first guess,²⁴ need not be a fully adequate form for values of $c \sim 1$, which imply a considerable amount of coherence. (The exponential memory function gives results that are qualitatively similar to the Gauss-

ian, when larger values of τ_s/τ_R are used.) Thus it may not be unreasonable to expect that a more satisfactorily chosen memory function, based on the correct molecular dynamics, would be in better agreement with our observations.

IV. RESULTS AND ANALYSIS: SATURATION

A. Saturation Measurements in the Motional-Narrowing Region

The experimental values for $T_1^{-1}(\bar{M})$ for PADS in 50% and 85% glycerol-H₂O are given in Table IV. T_1 results for PADS in H₂O have been given by Kooser *et al.*³ The absolute uncertainty in the T_1 values in Table IV is about 20% due mainly to uncertainty in the absolute value of Q and the proportionality constant in Eq. (2.1). The measured variation of $T_1(\bar{M})$ amongst the hyperfine components at a given temperature (and τ_R) is independent of the absolute value of B_1^2 , and the uncertainty in $T_1^{-1}(\pm 1)/T_1^{-1}(0)$ varies from 4% to 7%. The relative uncertainty among T_1 values for the same sample at different temperatures is 7%–10% due to the additional uncertainty in the temperature dependence of Q .

A preliminary analysis of the data in Table IV shows that T_1 is a slowly varying function of τ_R . Thus while $T_2^{-1}(0)$ increases by a factor of 10 from $\tau_R = 3 \times 10^{-11}$ sec to 1×10^{-9} sec, $T_1^{-1}(0)$ decreases by only $\sim 30\%$ over the same τ_R range. The data in Table IV also indicates that within experimental error T_1 is correlated with τ_R but not with the precise glycerol-H₂O composition.

The analysis of the saturation results in terms of the pseudosecular and nonsecular dipolar and g -tensor terms and the spin-rotational terms is relatively straightforward. One defines a saturation

TABLE IV. Fast motional saturation.

| A. Saturation Results for 50% Glycerol-H ₂ O | | | | | | |
|---|-----------------------------|--|-------|---|------------------------------|------------------------------|
| $T(^{\circ}\text{C})$ | $\tau_R \times 10^{11}$ sec | $T_1^{-1}(0) \times 10^{-6}$ sec ⁻¹ | b^a | $W_e(0) \times 10^{-5}$ sec ⁻¹ | $T_1^{-1}(-1)/T_1^{-1}(0)^b$ | $T_1^{-1}(+1)/T_1^{-1}(0)^b$ |
| 0 | 3.00 | 1.22 | 0.24 | 3.65 | 0.85 ± 0.03(0.85, 0.86) | 0.98 ± 0.04(1.03, 0.93) |
| -8 | 4.92 | 1.23 | 0.48 | 3.02 | 0.75 ± 0.05(0.79, 0.82) | 0.86 ± 0.04(0.94, 0.87) |
| -16 | 8.98 | 1.21 | 1.1 | 2.35 | 0.78 ± 0.04(0.75, 0.79) | 0.87 ± 0.04(0.85, 0.82) |
| -24 | 16.5 | 1.18 | 2.5 | 1.98 | 0.80 ± 0.03(0.78, 0.81) | 0.83 ± 0.03(0.84, 0.83) |
| -30 | 31.7 | 1.02 | 5.5 | 1.62 | 0.88 ± 0.03(0.86, 0.87) | 0.89 ± 0.03(0.88, 0.88) |
| B. Saturation results for 85% Glycerol-H ₂ O | | | | | | |
| $T(^{\circ}\text{C})$ | $\tau_R \times 10^{10}$ sec | $T_1^{-1}(0) \times 10^{-6}$ sec ⁻¹ | b^a | $W_e(0) \times 10^{-5}$ sec ⁻¹ | $T_1^{-1}(-1)/T_1^{-1}(0)^b$ | $T_1^{-1}(+1)/T_1^{-1}(0)^b$ |
| 18 | 1.64 | 1.28 | 2.1 | 2.27 | 0.78 ± 0.03(0.78, 0.80) | 0.80 ± 0.05(0.83, 0.81) |
| 10 | 2.53 | 1.30 | 3.4 | 2.24 | 0.78 ± 0.05(0.82, 0.83) | 0.89 ± 0.06(0.85, 0.84) |
| 3 | 4.16 | 1.09 | 7.0 | 1.77 | 0.83 ± 0.03(0.88, 0.88) | 0.84 ± 0.04(0.90, 0.89) |
| -2 | 7.33 | 1.03 | 13 | 1.69 | 1.04 ± 0.03(0.92, 0.93) | 1.00 ± 0.05(0.93, 0.93) |
| -7 | 11.8 | 0.836 | 24 | 1.35 | 1.01 ± 0.05(0.96, 0.96) | 1.06 ± 0.05(0.96, 0.96) |

^a $b = W_N/W_e(0)$, where $2W_N$ is the nuclear spin-flip rate.

^b Numbers in parentheses are calculated from Eq. (4.1) utilizing $\epsilon = 1$ and 4, respectively.

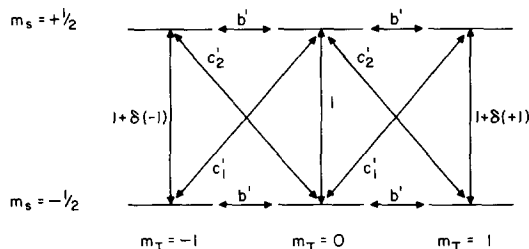


FIG. 7. Relaxation diagram for an $I=1$, $S=\frac{1}{2}$ spin system in which the different transition probabilities are defined in units of $W_e(0)$.

parameter $\Omega(\vec{M}) = 4T_1(\vec{M})$ which obeys

$$\Omega(\vec{M}) = 2C_{\vec{M},\vec{M}}/C_i, \quad (4.1)$$

where C_i and $C_{\vec{M},\vec{M}}$ are respectively any single cofactor and the double cofactor (for the \vec{M} transition) of the transition-probability matrix \mathbf{W} .^{8,16} The transition probabilities are defined in Fig. 7 as dimensionless quantities relative to $W_e(0)$, the pure electron-spin-flip rate of the $\vec{M}=0$ line, and they are detailed elsewhere.¹⁶ When the nonsecular dipolar terms are small compared to $W_e(0)$ (the usual case for $\omega_0\tau_R > 1$), then one obtains a relatively simple expression⁸

$$T_1^{-1}(\vec{M}) = 2W_e(0)\varphi^{-1}(\vec{M}), \quad (4.2)$$

$$\varphi(\pm 1) = (1 + 3b + b^2)/(1 + 4b + 3b^2), \quad (4.3a)$$

$$\varphi(0) = (1 + 2b + b^2)/(1 + 4b + 3b^2), \quad (4.3b)$$

and $b = \frac{1}{2}b'$. For $b \ll 1$, the pure nuclear-spin transitions are negligible, and each allowed transition relaxes independently with $T_1^{-1}(\pm 1) = T_1^{-1}(0) = 2W_e(0)$. For $b \gg 1$, the nuclear-spin levels are "shorted" and $T_1^{-1}(\pm 1) = T_1^{-1}(0) = 6W_e(0)$. When nonsecular terms are not negligible, one has a simple result for b' , c'_1 , $c'_2 \ll 1$,²⁶

$$\Omega(M) \approx [2/W_e(0)]\{1 - \delta(M) - [I(I+1) - M^2]S\}, \quad (4.4)$$

where

$$S = (b' + c'_1)(b' + c'_2)/(2b' + c'_1 + c'_2) \quad (4.5)$$

so that $T(1) \neq T(-1)$.

Although Eqs. (4.2)–(4.4) give useful approximate results, we used the general expressions based on Eq. (4.1) and Fig. 7, which are valid over the whole motional narrowing region.

It is possible to calculate values for $W_e(0)$ from the $T_1^{-1}(0)$ results, using Eq. (4.1) and the values for τ_R and N calculated from the relative linewidths of the unsaturated spectra. The procedure involves varying the value of $W_e(0)$ until the experimentally observed value of $T_1^{-1}(0)$ is obtained.

In the region where nonsecular terms are impor-

tant the value of $T_1^{-1}(0)/W_e(0)$ and $T_1^{-1}(\pm 1)/T_1^{-1}(0)$, for a given value of τ_R and N , depends on the functional form of $j(\omega_0, \tau_R)$. Thus a comparison of the experimental values of $T_1^{-1}(\pm 1)/T_1^{-1}(0)$ with those predicted from Eq. (4.1) should, in principle, be able to distinguish between the nonsecular contribution predicted for different values of ϵ in Eq. (3.3). Unfortunately, the experimental results are not accurate enough to distinguish between the use of $\epsilon = 1$ or $\epsilon = 4$ as shown in Table IV. The error in calculating $W_e(0)$, due to the uncertainty in the magnitude of the nonsecular dipolar (and g -tensor) terms due to uncertainty in ϵ , varies from $\sim 15\%$ for $\tau_R = 3 \times 10^{-11}$ sec to ~ 0 for $\tau_R > 3 \times 10^{-10}$ sec. The values of $W_e(0)$ and $T_1^{-1}(\pm 1)/T_1^{-1}(0)$, given in Table IV, were calculated using the equations relating the transition probabilities to the appropriate spectral densities, and are given in Refs. 8 and 22 for isotropic motion, but are easily modified for anisotropic motion.^{9,16} The calculated results for $T_1^{-1}(\pm 1)/T_1^{-1}(0)$, in general, agree with those found experimentally and support the validity of the saturation analysis. (However, there is some discrepancy for $\tau_R > 5 \times 10^{-10}$ sec.)

The variation of $W_e(0)$ with τ_R and $1/T$ is shown in Figs. 8 and 9 for 0, 50, and 85% glycerol–H₂O. The values of $W_e(0)$ for H₂O were obtained from the linewidths in Fig. 4 and the observation of Kooser *et al.* that $T_2^{-1} = T_1^{-1} = 2W_e(0)$ for PADS in this solvent.³ A least-squares fit to the log–log plot of $W_e(0)$ versus τ_R for PADS in H₂O yields

$$W_e(0) = 0.052\tau_R^{-0.64 \pm 0.02}. \quad (4.6)$$

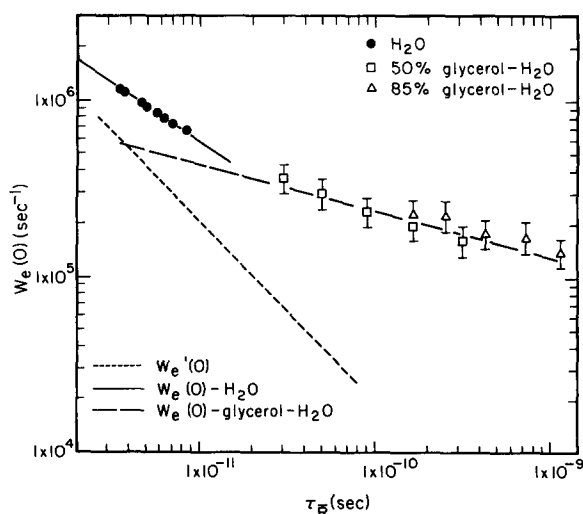


FIG. 8. $W_e(0)$ vs τ_R for PADS in glycerol–H₂O. Experimental values for H₂O, 50% glycerol–H₂O, and 85% glycerol–H₂O are designated by \bullet , \square , and \triangle , respectively. — and — — are least-squares fits to the experimental values. - - - is the difference between the two least-squares fits.

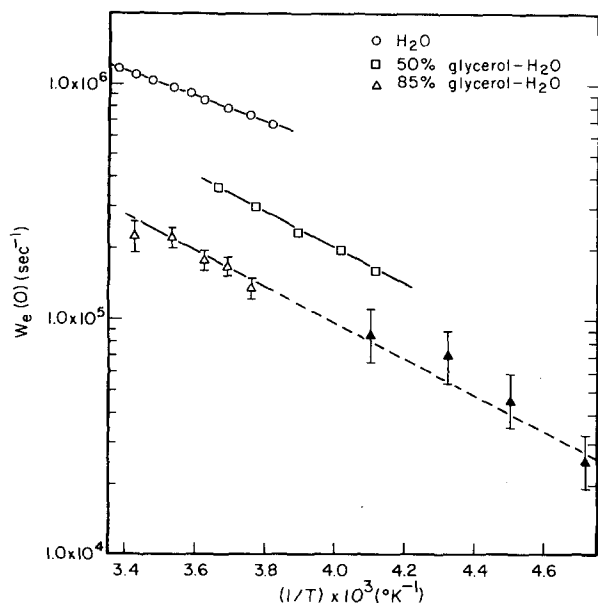


FIG. 9. $W_e(0)$ vs $1/T$ for PADS in glycerol- H_2O , motional-narrowing results for H_2O , 50% glycerol- H_2O and 85% glycerol- H_2O are designated by \circ , \square , and Δ , respectively. The slow-motional results for 85% glycerol- H_2O are designated by \blacktriangle . The lines are least squares fits to the motional narrowing results.

If $W_e(0)$ in this region is attributed to spin-rotation,²⁷ then one usually expects that $W_e(0) \propto 1/\tau_R$.

A least-squares fit to the results for 50 and 85% glycerol- H_2O yields

$$W_e(0) = 8.4 \times 10^2 \tau_R^{-0.25 \pm 0.03} \quad (4.7)$$

In this region $W_e(0)$ is a very slowly varying function of τ_R . This is significantly different from the results for H_2O and indicates that either $W_e(0)$ results from a single mechanism (e.g., spin-rotation) which is a complicated function of τ_R , or else there are two independent relaxation processes that are contributing to $W_e(0)$. Note that if Eq. (4.7) is extrapolated to shorter τ_R and subtracted from Eq. (4.6), then the residual $W_e'(0) \propto \tau_R^{-1.1 \pm 0.3}$, which is the expected result for the usual spin-rotational relaxation:

$$W_e^{SR} = \sum (g_i - g_s)^2 / 18 \tau_R, \quad (4.8a)$$

where we have used

$$\tau_J = (I/6kT) \tau_R^{-1} \quad (4.8b)$$

and the value of $W_e'(0) = 5.7 \times 10^5 \text{ sec}^{-1}$ for $\tau_R = 3.5 \times 10^{-12}$ compares well to $7.1 \times 10^5 \text{ sec}^{-1}$ from Eq. (4.8). If Eq. (4.7) results from another spin-relaxation mechanism, then it is interesting to note from Fig. 7 that it predominates for $\tau_R > 3 \times 10^{-11}$ sec or for about the same range that the anomalous residual portion of the linewidth (cf. Fig. 5) is im-

portant. The alternative possibility that both the anomalous T_2 and W_e behavior for $\tau_R > 3 \times 10^{-11}$ sec is due to unusual features in the spin-rotational relaxation cannot be entirely ruled out. Thus, for example, we note that Krynicki and Powles²⁸ have found from their analysis of proton NMR T_1 data in HCl, that τ_J , the spin-rotational correlation time is nearly constant for $T < 0^\circ \text{C}$ even increasing slightly instead of the expected $\tau_J \propto \tau_R^{-1} \propto T/\eta$. This curvature is not entirely unlike our results for $W_e(0)$ in Fig. 9, but we cannot justify the large discrepancy between $2W_e(0)$ and the residual A behavior for $\tau_R > 3 \times 10^{-11}$ sec, which is of the type implying that nonsecular contributions are weaker than secular ones.²⁹

The temperature dependence of W_e for PADS in aqueous glycerol solutions is given in Fig. 9. For 0%, 50%, and 85% glycerol- H_2O solutions, the "activation energy" is 2.5 ± 0.1 , 3.5 ± 0.1 , and 3.2 ± 0.6 kcal/mole, respectively. The results for 50% and 85% glycerol- H_2O can be compared to the 10.4 ± 0.2 and 11.3 ± 0.1 kcal/mole activation energy obtained for reorientation (cf. I). Thus for these two solvents, the "activation energy" for W_e , within experimental error, is independent of glycerol- H_2O composition and substantially smaller than for reorientation. These results suggest that if W_e does

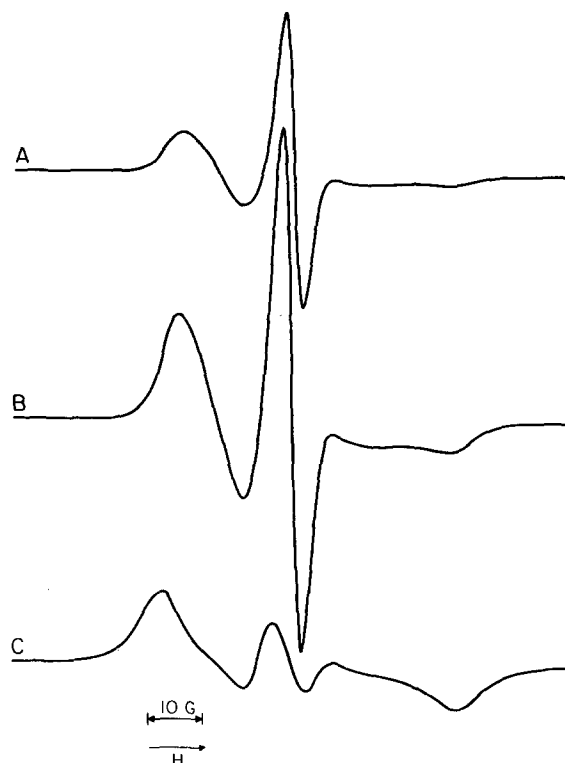


FIG. 10. Experimental spectra for PADS in 85% glycerol- H_2O at $T = -29^\circ \text{C}$ and (A) $d_e = 0.026$ G, (B) $d_e = 0.083$ G, and (C) $d_e = 0.45$ G.

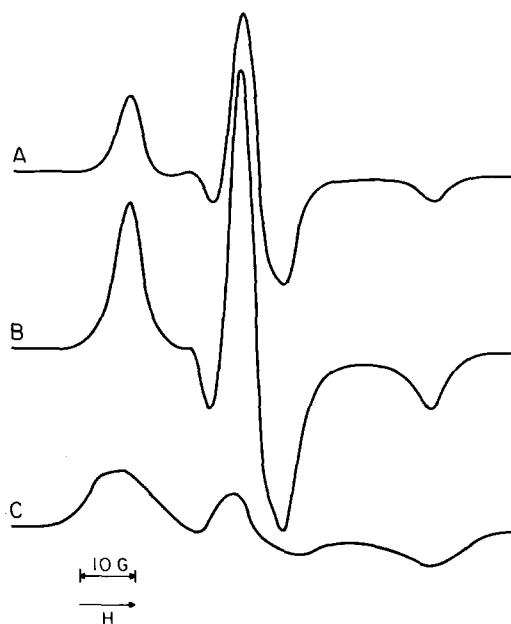


FIG. 11. Experimental spectra for PADS in 85% glycerol-H₂O at $T=61^\circ\text{C}$ and (A) $d_e=0.019$ G, (B) $d_e=0.061$ G, and (C) $d_e=0.45$ G.

originate from a spin-rotational interaction, then changes in the angular momentum associated with the short time (and less restricted) behavior of the reorientation may contribute to the spin relaxation. Thus, for example, perhaps angular momentum fluctuations associated with torsional oscillations could result in an appreciable spin-rotational relaxation even when the reorientational motion is effectively retarded by the large solvent viscosities.

The values of W_e obtained from the analysis of the saturated slow-motional line shapes (cf. Sec. IV B) are in good agreement with the extrapolated W_e versus $1/T$ results for 85% glycerol-H₂O as shown in Fig. 9. This indicates that the mechanism for electron spin flips remains unchanged even for reorientation as slow as $\tau_R \approx 2 \times 10^{-7}$ sec.

B. Saturation in the Slow-Motional Region

Saturation studies were performed on PADS in 85% glycerol-H₂O for $-29^\circ\text{C} > T > -93^\circ\text{C}$. In this temperature range, τ_R was estimated by extrapolating the least-squares fit of τ_R vs $1/T$ (cf. Fig. 10 of I) for the motional-narrowing region, to lower temperatures. These τ_R values are given in Table IV. Within experimental error, these extrapolated τ_R values agree with those obtained from the method described in Ref. 4 based on simulations of unsaturated slow-tumbling spectra. Selected saturated line shapes are shown in Figs. 10-12 for $T = -29$, -61 , and -93°C , respectively. A comparison of the saturated versus unsaturated experimental

spectra indicate that the general features of the saturated spectra are very sensitive to the microwave field strength and the rotational correlation time. For $T \geq -61^\circ\text{C}$, the effect of increasing the microwave power is to first maximize the center line, then the low field extrema and finally the high field extrema of the slow-motional spectra. At large microwave field strengths (e.g., $d_e = 0.45$ G, see below, or 350 mW with $Q \approx 7800$), the observed spectra (cf. curves C) are dominated by the outer hyperfine extrema, while the central region is almost completely saturated. This contrasts greatly with the unsaturated spectra at these temperatures (cf. curves A). For $T = -93^\circ\text{C}$, the spectrum saturated more uniformly and, within experimental error, the central region and the outer hyperfine extrema maximize at the same microwave power. These results can be expressed quantitatively in terms of $d_{\max}(\bar{M})$. Here \bar{M} of -1 , 0 , and $+1$ correspond to the low field extrema, central region, and high field region, respectively, while $d_e = \frac{1}{2} |\gamma_e| B_1$ and d_{\max} gives the microwave field strength at which these regions of the spectra maximize. The variation of $d_{\max}(+1)/d_{\max}(-1)$ and $d_{\max}(+1)/d_{\max}(0)$ with τ_R is given in Fig. 13, while curves B of Figs. 10-12 are for $d_{\max}(0)$. The value of $d_{\max}(+1)/d_{\max}(0)$ and $d_{\max}(+1)/d_{\max}(-1)$ vary from 3.2 ± 0.3 and 1.8 ± 0.2 for $\tau_R = 9.4 \times 10^{-9}$ sec to ~ 1 for $T = -93^\circ\text{C}$ and $\tau_R \sim 4 \times 10^{-5}$ sec. A comparison of the results for

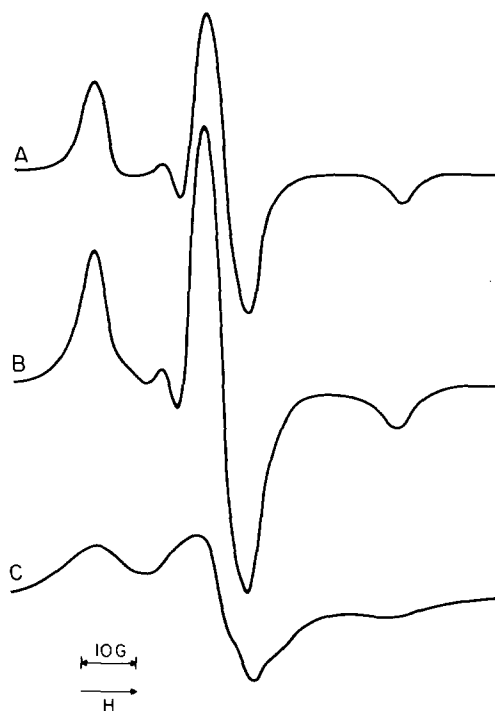


FIG. 12. Experimental spectra for PADS in 85% glycerol-H₂O at $T = -93^\circ\text{C}$ and (A) $d_e = 0.0041$ G, (B) $d_e = 0.013$ G, and (C) $d_e = 0.45$ G.

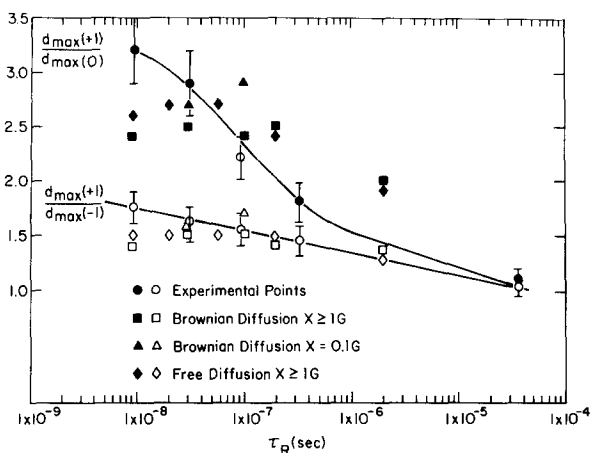


FIG. 13. Variation of $d_{\max}(+1)/d_{\max}(0)$ and $d_{\max}(+1)/d_{\max}(-1)$ with τ_R . Solid lines are drawn through the experimental points.

$T = -61^\circ\text{C}$ ($\tau_R = 3 \times 10^{-7}$ sec) and $T = -93^\circ\text{C}$ indicate that the saturated ESR line shapes and the relative values of $d_{\max}(\vec{M})$ differ even though their unsaturated spectra are virtually superimposable. Thus it could be possible to utilize the relative values of d_{\max} , as shown in Fig. 13 as a means to determine τ_R for longer correlation times than is possible from τ_R dependent variations of the unsaturated line shape.

In order to analyze the results in Figs. 10–13, etc. the experimentally observed spectra for PADS were compared to simulated saturated slow-motional line shapes calculated using the methods developed in I, but extended for the simulation of saturated $I = 1$, $S = \frac{1}{2}$ nitroxide spectra (cf. Appendix A). In order to minimize computer time the dipolar and g tensors were taken to be axially symmetric, and isotropic reorientation was assumed (although complete expressions, not involving these assumptions, are given elsewhere).³⁰ The model dependence of the reorientation was introduced in the same manner as I while an orientation-independent W_e was generally assumed, and it was further assumed that W_n would be predominantly due to the pseudosecular dipolar terms explicitly included, so that no appreciable intrinsic W_n term had to be introduced, (cf. Appendix A).

Saturated slow-motional nitroxide spectra were simulated for both Brownian and free diffusion reorientation models for a variety of cases.¹⁶ Typical spectra simulated for Brownian diffusion with τ_R of 9×10^{-9} sec are shown in Fig. 14, while free diffusion (or equivalently moderate jump) simulations are shown in Fig. 15. For these calculated line shapes, the residual Lorentzian first derivative width was chosen to approximately match the experimentally observed glycerol–H₂O widths. The ini-

tial choice of W_e was based on the extrapolation of the least-squares fit of W_e versus τ_R for 85% glycerol–H₂O in Fig. 8. A, B, and C in each figure correspond to microwave field strengths of $d_e \ll d_{\max}(0)$, $d_e \approx d_{\max}(0)$, and $d_e \gg d_{\max}(0)$, respectively. Comparisons of simulated with observed spectra (e.g., Fig. 10 vs Figs. 14 and 15), indicate that the general features of curves for both the Brownian and free diffusion models are very similar to the corresponding experimental spectra. The spectral features of the simulated spectra that are associated with the model dependence of the reorientation are broadened at large microwave field strengths. Thus the qualitative characteristics of the line shape are only model dependent for unsaturated or weakly saturated spectra. Since the approximation of an axial g -tensor and isotropic reorientation does affect the detailed simulated line shapes, the calculated and experimental spectra do show differences in a detailed comparison.

The variation of $d_{\max}(+1)/d_{\max}(0)$ and $d_{\max}(+1)/d_{\max}(-1)$ with τ_R for the simulated line shapes is given in Fig. 13 for Brownian and free diffusion with 9×10^{-9} sec $< \tau_R < 2 \times 10^{-6}$ sec. The calculated results show, in general, reasonable agreement with the experimental ones considering our approx-

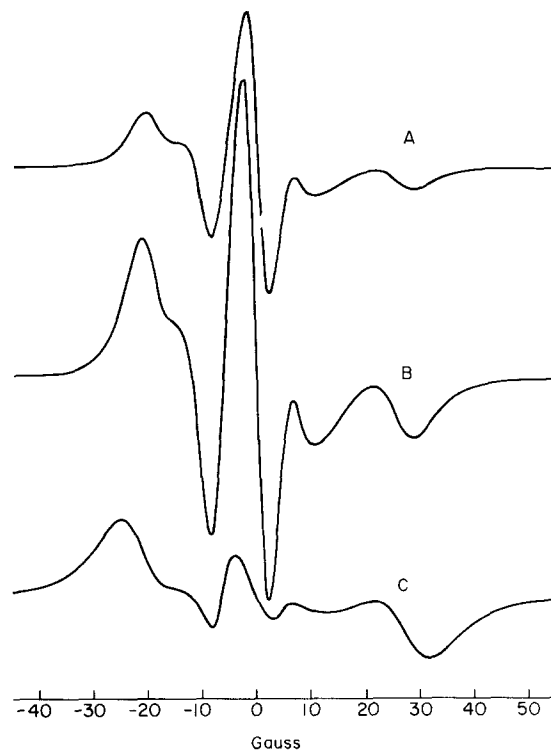


FIG. 14. Slow-motional spectra simulated for Brownian diffusion with $\tau_R = 9 \times 10^{-9}$ sec, $X = 1.0$ G, $W_e = 8.8 \times 10^4$ sec⁻¹, and (A) $d_e = 0.03$ G, (B) $d_e = 0.10$ G, and (C) $d_e = 0.47$ G. To be compared with the experimental results in Fig. 10.

imations. For $\tau_R \lesssim 2 \times 10^{-8}$ sec, the calculated values of $d_{\max}(+1)/d_{\max}(0)$ and $d_{\max}(+1)/d_{\max}(-1)$ for Brownian and free diffusion models are somewhat smaller than the values observed experimentally. For $d_{\max}(+1)/d_{\max}(0)$, good agreement with the experimental results is obtained for some of the calculations in the region 2×10^{-8} sec $< \tau_R < 1 \times 10^{-7}$ sec. For $\tau_R > 1 \times 10^{-7}$ sec, however, the calculated value of $d_{\max}(+1)/d_{\max}(0)$ again differs somewhat from the experimentally observed results. The agreement for $d_{\max}(+1)/d_{\max}(-1)$ is somewhat better, with good agreement for $\tau_R > 2 \times 10^{-8}$ sec. The saturation behavior of these spectra does not exhibit any significant model dependence. This suggests that the $d_{\max}(\bar{M})$ values are determined more by τ_R than by the specific model for τ_R .

One obvious reason for the discrepancy between experimental and calculated values for $d_{\max}(\bar{M})/d_{\max}(\bar{M}')$ for certain τ_R values is the approximation of an axial g -tensor and isotropic reorientation. These simplifying assumptions affect the line shape and widths of the entire spectrum for $\tau_R \lesssim 2 \times 10^{-8}$ sec and the shape of the central region of the spectrum for $\tau_R \gtrsim 2 \times 10^{-8}$ sec. For these longer τ_R values, the shape of the outer hyperfine extrema is virtually independent of the g -tensor values (cf. I). For the overlapped central region of the spectrum,

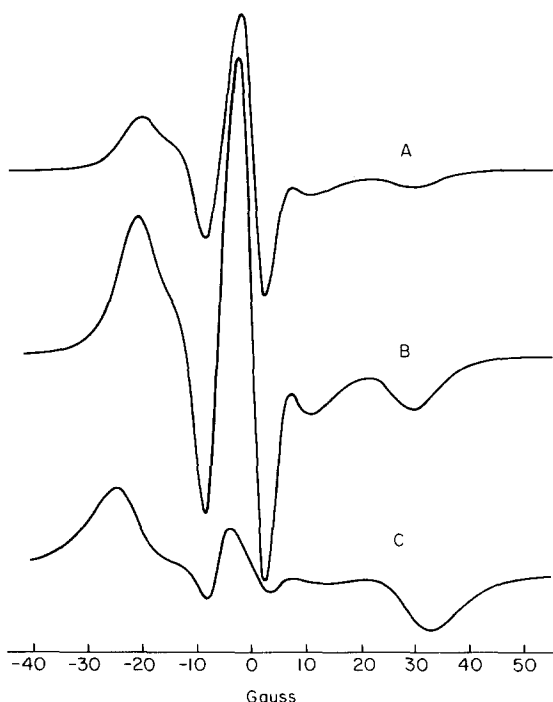


FIG. 15. Slow-motional spectra simulated for free diffusion with $\tau_R = 9 \times 10^{-9}$ sec, $X = 1.0$ G, $W_e = 8.8 \times 10^4$ sec $^{-1}$, and (A) $d_e = 0.03$ G, (B) $d_e = 0.10$ G, and (C) $d_e = 0.47$ G. To be compared with the experimental results in Fig. 10.

the relative peak-to-peak derivative width of the experimental and simulated spectra varies with τ_R . For $\tau_R = 9 \times 10^{-9}$ sec, the center line of the unsaturated spectrum simulated for free diffusion is about 0.6 G or 16% broader than the comparable experimental spectrum. The width difference increases to about 1 G or 25% broader for free diffusion and $\tau_R = 2 \times 10^{-8}$ sec. For longer τ_R values, however, the experimental width of the center line increases more rapidly than the comparable width for the simulated line shapes. For $\tau_R = 2 \times 10^{-6}$ sec, the peak-to-peak derivative width of the asymmetric center line of the experimental unsaturated spectrum is 8 G. For the simulated spectrum, the over-all spread of the central region is about 8 G, but there is some resolvable structure to the center line. The narrower lines result from the decreased overlap due to the assumed axial symmetry versus an experimental asymmetric g tensor. Thus the effective width of the central region is smaller for the simulated versus experimental spectra for long τ_R .

It is expected that these width and line shape differences will affect the detailed saturation behavior of the simulated versus experimental line shapes and the relative values of $d_{\max}(+1)/d_{\max}(0)$. For a first derivative Lorentzian line shape, for example,

$$d_{\max}^2 = (C) T_1^{-1} T_2^{-1} \quad (4.9)$$

(with $C = \frac{1}{8}$) and d_{\max} varies as the square root of the linewidth. The agreement between the experimental and calculated values of $d_{\max}(+1)/d_{\max}(-1)$ for $\tau_R \gtrsim 2 \times 10^{-8}$ sec indicates that the predictions of the saturation theory are accurate in the regions of the spectrum where the contributions of the g -tensor components are insignificant. The agreement between the experimental and calculated $d_{\max}(+1)/d_{\max}(0)$ ratios over the range of τ_R values where the over-all line shape of the simulated and experimental spectra are closest suggests that the lack of complete agreement for other τ_R values is due to the obvious line shape differences between the spectra.

The effect of varying X , the residual width, on the calculated values of $d_{\max}(\bar{M})$ was examined for two τ_R values. For Brownian diffusion and $\tau_R = 3 \times 10^{-8}$ sec, spectra were simulated for $X = 1.2$ and 0.1 G. This corresponds to a 20% decrease in the over-all width of the $\bar{M} = 0$ line. The 4 G derivative width for the latter is the same as the experimental $\bar{M} = 0$ width for $T = -41$ °C. The 10% decrease observed in the calculated $d_{\max}(0)$ is consistent with Eq. (4.9) even though the shape of the $\bar{M} = 0$ line deviates from a Lorentzian for this values (cf. Fig. 15). For the 0.1 G residual width, the experimental and calculated values of $d_{\max}(+1)/d_{\max}(0)$ and $d_{\max}(+1)/d_{\max}(-1)$ agree within experimental error

(cf. Fig. 13). A similar variation of $d_{\max}(0)$ with X is observed for longer τ_R values. When X is decreased from 2 to 0.1 G for Brownian diffusion and $\tau_R = 1 \times 10^{-7}$ sec, the values of $d_{\max}(0)$, $d_{\max}(-1)$, and $d_{\max}(+1)$ decrease by 20%, 10%, and $\sim 0\%$, respectively. The 20% decrease in $d_{\max}(0)$ is consistent with Eq. (4.9) and the approximate 33% decrease of the peak-to-peak derivative width of the center line. For this value of τ_R , these changes in d_{\max} do not improve the agreement in Fig. 13. These results indicate that Eq. (4.9) where the peak-to-peak derivative width is substituted for T_2^{-1} , can be used to approximately describe the linewidth dependence of $d_{\max}(0)$.

The effect of varying W_e and the residual width X on the calculated values of d_{\max} was also examined. The dependence of $d_{\max}(\bar{M})$ on W_e can approximately be fit to

$$d_{\max}^2(\bar{M}) = C(\bar{M}) W_e(0), \quad (4.10)$$

where $C(\bar{M})$ is a constant for a given value of τ_R and X . [This relation is similar to the saturation behavior of a motionally narrowed first derivative line cf. Eq. (4.9).] Within the error of the calculation, the ratios of the $d_{\max}(\bar{M})$ are not affected by reasonable changes in W_e .

It should be noted that for long τ_R , i. e., $\tau_R > 1 \times 10^{-7}$ sec, the residual width is largely due to inhomogeneous broadening mainly from unresolved electron-solvent dipolar interactions and from site variations in the magnetic tensors. In the simulated spectra, the residual width is treated as a homogeneous broadening. Thus for $\tau_R = 1 \times 10^{-7}$ sec, where the residual width is on the order of twice the motional width arising from time-dependent modulation of $\mathcal{H}_1(\Omega)$, neither the assumption of $X = 2$ or 0.1 G accurately describes the experimental spectra. Due to the fact that an inhomogeneously broadened line saturates differently from a homogeneously broadened line of the same width, a better analysis for long τ_R should be achieved by convoluting the line shapes obtained from our slow-tumbling analysis, with a shape function representing the inhomogeneous broadening in the usual manner.^{30a}

While the slow-tumbling saturation expressions are complex (cf. Ref. 30) and hence not easily amenable to analysis, there are some relevant features which may be seen from the much simpler expressions for a single-line spectrum (cf. II). In this case the effect of W_e and d_e^2 appears only in the term: $4d_e^2/[2W_e + L(L+1)B_L R]$ for each coefficient (i. e., the $C_{R,M}^L$ of Appendix A) corresponding to a different value of L (where B_L is the model parameter, cf. I). This expression for $L=0$ is just the normal one for saturation of a motionally narrowed line. As the different coefficients of $L > 0$

are coupled in due to the slowed motion, the full denominator becomes important. In fact for $\tau_R^{-1} = 6B_L R > 2W_e$, which is always true in the present study, the effect of W_e is negligible except for the $L=0$ term. It appears, therefore, from Eq. (4.10) that the dominant saturation behavior is determined by the behavior of the $L=0$ coefficients in the region of $d_e(\max)$. The model parameter B_L which ranges from unity to $[L(L+1)]^{-1}$, depending upon model (cf. I), should have marginal effect on the saturation behavior, beyond its general effects on the unsaturated spectrum, as it deviates from a Brownian motion value of $B_L = 1$, viz., to cause a more rapid onset of slow-tumbling as τ_R increases. (Further points, based on a careful analysis of the complete equations, are made in Appendix A.)

However, one might wish to introduce an orientation-dependent W_e to try to explain a discrepancy for $\tau_R > 2 \times 10^{-7}$ sec. In particular one might let $W_e = A + B \cos^2 \theta$, where θ is the polar angle; then in the rigid limit, the central region of the spectrum, associated with the x and y molecular axes parallel to $B_0(\theta = \pi/2, W_e = A)$ would have a different W_e than the outer extrema, which are associated with the z -molecular axis parallel to $B_0(\theta = 0, W_e = A + B)$. The simple use of Eq. (4.9) and Fig. 13 would suggest that for $\tau_R = 2 \times 10^{-7}$ sec, $B \approx -A/3$. However, this approach appears inadequate on two counts: (1) the discussion in Appendix B for orientation-dependent spin-rotational relaxation shows that W_e^{SR} should be about twice as great for $\theta = 0$ as for $\theta = \pi/2$, or the reverse of the observed trend, as a result of the fact that $g_{zz} - g_e \approx 0$; however even more significantly: (2) the orientation-dependent term $B \cos^2 \theta$ would still be expected to average out as long as $W_e \tau_R \ll 1$ (note $W_e \tau_R \approx 7 \times 10^{-3}$ for $\tau_R = 2 \times 10^{-7}$) by virtue of the fact that it would only couple coefficients of different L value (i. e., it gives off-diagonal matrix elements of \mathcal{A} in Eq. (A6) of Appendix A, while the relevant diagonal elements go as $L(L+1)B_L R$).³¹

The possible effects of nonnegligible, intrinsic W_n 's as well as those of short-time nondiffusive effects on the nuclear-spin-flip transitions induced by the dipolar terms when $\tau_R^{-1} \lesssim |\gamma_e| a_N$ (by analogy with the possible short-time nondiffusive effects on nonsecular terms when $\omega_e \tau_R \gtrsim 1$ discussed in Sec. III) has yet to be considered. Note however, that for $W_n \tau_R \ll 1$, only the orientation invariant or average values of W_n would be needed (for the same reason as that for W_e given above).

The above comments must remain somewhat uncertain until accurate simulations are performed for an asymmetric nitroxide with inhomogeneous line broadening and more work is done for longer τ_R values. Additional experiments on a completely

deuterated system would also be useful since it would reduce somewhat the ambiguity resulting from the presence of inhomogeneous line broadening. However, the semiquantitative agreement that is obtained for the PADS system demonstrates the applicability of this approach to the interpretation of saturated ESR line shapes in terms of reorientational and spin relaxation parameters.

The above complications notwithstanding, it is still possible to estimate W_e in the slow-motional region from the experimental saturation results. When Eq. (4.9) is employed, a comparison of $d_{\max}(\vec{M})$ versus τ_R for the simulated and experimental line shapes gives a value of W_e for each region of the experimental spectrum. The average of these three values for results in the range of $T = -29$ to -61°C is given in Fig. 9. Within the approximately $\pm 30\%$ error in the calculation, the calculated values of W_e in the slow-motional region agree with the extrapolated least square fit of $W_e(0)$ vs $1/T$ for 85% glycerol-H₂O in the motional-narrowing region.

V. SUMMARY AND CONCLUSIONS

One of the main results of this work has been to demonstrate that saturation studies may be effectively extended from the motional narrowing region to the slow-tumbling region. By means of the stochastic-Liouville method we have been able to predict spectra as a function of microwave power which have the same general features as those observed experimentally, even though, for convenience in this work, we used the approximations of an axially symmetric g -tensor, isotropic rotational reorientation, and homogeneous intrinsic widths. We have been able to extract out a rotationally invariant W_e in the slow-motional region and have found that our results agree with the values of W_e extrapolated from the motional-narrowing region. Also our analysis implies that as long as $W_e\tau_R \ll 1$, any orientation-dependent contributions to W_e should have its effects averaged out. The observed variations in the relative saturation behavior for different portions of the spectrum as a function of τ_R were only approximately reproduced in our analysis, presumably largely due to our simplifying assumptions. But such variations should potentially be useful in extending the range over which τ_R is measurable to longer values. On the other hand, we have found from our analysis that slow-tumbling saturation studies are not useful for obtaining information about models of rotational reorientation: the saturated line shapes become less sensitive to model dependence than the unsaturated shapes, and the use of a moderate jump or a free-diffusion model in place of a Brownian motion model does not significantly alter the results obtained for W_e or the relative saturation behavior of different regions

of the spectrum.

The motional-narrowing saturation results were successfully analyzed in terms of the proper motional-narrowing theory yielding also generally good agreement with the variation in T_1 amongst the hyperfine lines. These results for glycerol-H₂O solvent including those in the slow-tumbling region show that W_e is only a weak function of τ_R (i. e., $\tau_R^{-1/4}$) although in aqueous solvent W_e depends more strongly on τ_R . This observation has been discussed in terms of spin-rotational relaxation, although no definite conclusions were reached.

The studies of the motional-narrowing unsaturated line shapes for PADS in a variety of glycerol-H₂O solvents for X-band as well as a study at 35 GHz and a study of ¹⁷O-labeled PADS supplied us with several independent checks on our results for τ_R and N , the ratio of the two components of the axially symmetric diffusion tensor. (None of the experiments proved to be sensitive to deviations from axial symmetry.) Excellent agreement was achieved for the results of the different experiments (yielding $N \approx 4.7$), thus enhancing our conviction about the effectiveness and accuracy of obtaining such information on rotational motion in liquids by ESR techniques. However, these experiments demonstrated that for $\tau_R \sim \omega_0^{-1} = 1.7 \times 10^{-11}$ sec anomalous behavior, which could be attributed to the nonsecular spectral densities, does indeed occur. The results on ¹⁷O-labeled PADS, which could only be carefully studied for $\tau_R < 5 \times 10^{-12}$ sec, indicate, however, that for $(\omega_0\tau_R)^2 \ll 1$ the nonsecular spectral densities associated with the linewidth contribution due to ¹⁷O are no longer anomalous. Simple analyses of these results for the nonsecular spectral densities are given in terms of nondiffusive (or non-Markovian) behavior of the rotational motion. An analysis based on a simple model of inertial effects does not appear to "explain" our observations. However, a more phenomenological treatment based on the memory function (or relaxing cage) approach was found to be able to qualitatively reproduce some features by the use of large values for τ_G , the "cage-relaxation time for a Gaussian decay," i. e., $\tau_G \gg \tau_R$, implying large deviations from simple diffusive motion.

APPENDIX A: SLOW-TUMBLING-SATURATION SIMULATIONS

The general methods for simulation of saturated ESR spectra are discussed in II. We wish to outline here (1) the generalizations required for nitroxide spectra over a simple one-line ESR spectrum and (2) more efficient computational methods.³⁰

The energy levels are properly labeled in Fig. 4B of II and the resonance frequencies for the ESR allowed and forbidden transitions appear in Eqs.

(A1)–(A6) of I. In addition to these nine frequencies, NMR transition frequencies will be needed. [Their coefficients are coupled by the pseudosecular terms in $\mathcal{H}_1(\Omega)$ to the coefficients for the six eigenstates.] These frequencies are

$$\begin{aligned} \omega_{10} &\equiv \omega_{ab} = \omega_{ba} = \omega_n + b, \\ \omega_{11} &\equiv \omega_{b'a'} = -\omega_n + b, \\ \omega_{12} &\equiv \omega_{bc} = \omega_n + b, \\ \omega_{13} &\equiv \omega_{c'b'} = -\omega_n + b, \\ \omega_{14} &\equiv \omega_{ac} = 2\omega_n + 2b, \\ \omega_{15} &\equiv \omega_{c'a'} = -2\omega_n + 2b. \end{aligned} \quad (\text{A1})$$

The above equations label the transitions. ω_{ij} (e.g., ω_{ab}) refers to the transition frequency from level i to level j . Also ω_n is the NMR Larmour frequency due to the Zeeman term, and b is the hyperfine term. For axially symmetric g -tensor and electron-nuclear dipolar tensor, $\mathcal{H}_1(\Omega)$ the orientation dependent perturbation is given by Eq. (3.8) of I where nonsecular terms (S_2) have been neglected, while the more general expressions are given by Bruno.³⁰ The procedure now is to substitute the appropriate expressions for $\mathcal{H}_1(\Omega)$, into a generalized form of the expressions given in II for the stochastic-Liouville method as solved in terms of the normalized eigenfunctions $G_m(\Omega)$ (with eigenvalues τ_m^{-1}) of the rotational diffusion operator, [cf. Eqs. (48) and (53) of II]:

$$\begin{aligned} &[(n\omega - \omega_{\alpha\beta}) - i\tau_m^{-1}][C_m^{(n)}]_{\alpha\beta} + \sum_{m'} \int d\Omega G_m^*(\Omega) G_{m'}(\Omega) \\ &\times \{ \mathcal{H}_1(\Omega), C_m^{(n)} \}_{\alpha\beta} + d_e \{ [C_m^{(n+1)}]_{\alpha(-),\beta} - [C_m^{(n+1)}]_{\alpha,\beta(+)} \} \\ &+ d_e \{ [C_m^{(n-1)}]_{\alpha(+),\beta} - [C_m^{(n-1)}]_{\alpha,\beta(-)} \} \\ &= q\omega_{\alpha\beta} d_e \delta_{\alpha,\beta(-)} \delta_{n,1} \delta_{m,0}, \quad (\text{A2}) \end{aligned}$$

where $[C_m^{(n)}]_{\alpha\beta}$ refers to the expansion coefficient for the m th eigenfunction at the n th harmonic of the rf resonant field and is the matrix element between eigenstates α and β of \mathcal{H}_0 , the zero-order Hamiltonian. Also $d_e = \frac{1}{2} \gamma_e B_1$. Other definitions are as in I and II. The subscripts $\alpha(\pm)$ and $\beta(\pm)$ refer to states which differ from α , β by having their value of m_e raised (+) or lowered (-) by one. If no such state exists, the term is zero.

The effect of the radiation field is to require terms for harmonics $n=0$ and $n=1$ (cf. II). The pseudosecular terms in $\mathcal{H}_1(\Omega)$ result in the coupling of the $n=0$ NMR transition terms to the six ESR eigenstate terms (or the three eigenstate pair terms). Just as a rotationally invariant $T_{1,a}^{-1} = (2W_e)$ had been introduced into the two level system in II, a similar treatment may be used to include a rotationally invariant $T_{1,a}^{-1}(e) = 2W_e$ as well as a rotationally invariant $T_{1,a}^{-1}(n) = 2W_n$, where W_n

is the lattice-induced nuclear spin flip rate into the six level system. A proper analysis of the rotationally invariant W_e and W_n in terms of the transition-probability matrix⁸ shows that one may merely modify Eq. (A2) for $n=0$ by the following substitutions:

$$\tau_m^{-1} [C_m^{(0)}]_{aa} \rightarrow (\tau_m^{-1} + W_e + W_n) [C_m^{(0)}]_{aa} - W_e [C_m^{(0)}]_{a'a'} - W_n [C_m^{(0)}]_{bb}, \quad (\text{A3a})$$

$$\tau_m^{-1} [C_m^{(0)}]_{bb} \rightarrow (\tau_m^{-1} + W_e + 2W_n) [C_m^{(0)}]_{bb} - W_e [C_m^{(0)}]_{b'b'} - W_n [C_m^{(0)}]_{aa} - W_n [C_m^{(0)}]_{cc}, \quad (\text{A3b})$$

$$\tau_m^{-1} [C_m^{(0)}]_{cc} \rightarrow (\tau_m^{-1} + W_e + W_n) [C_m^{(0)}]_{cc} - W_e [C_m^{(0)}]_{c'a'} - W_n [C_m^{(0)}]_{bb} \quad (\text{A3c})$$

with the three additional expressions obtained by exchanging primed and unprimed subscripts (e.g., $a \rightarrow a'$ and $a' \rightarrow a$). In addition to these, the $n=0$ nuclear spin transition terms require the following substitutions:

$$\tau_m^{-1} [C_m^{(0)}]_{ij} \rightarrow (\tau_m^{-1} + W_e + T_{2,n}(0)^{-1}) [C_m^{(0)}]_{ij} - W_e [C_m^{(0)}]_{i'j'}, \quad (\text{A4})$$

where ij and $i'j'$ refer to the NMR transitions of Eqs. (A1). Again further needed substitutions are obtained by exchanging the primed and unprimed subscripts. It was shown in II that setting $\omega_n=0$ is an excellent approximation for simulating line shapes and it leads to considerable simplification of the equations. It is even more helpful for the saturation equations, because of their inclusion of the nuclear spin transitions. As a result of the symmetries one has only to consider the following linear combinations:

$$\overline{C}_{K,1}^{L(0)}(10, 11) = 2^{-1/2} [\overline{C}_{K,1}^{L(0)}(10) + \overline{C}_{K,-1}^{L(0)}(11)],$$

$$\overline{C}_{K,1}^{L(0)}(12, 13) = 2^{-1/2} [\overline{C}_{K,1}^{L(0)}(12) + \overline{C}_{K,-1}^{L(0)}(13)], \quad (\text{A5})$$

$$\overline{C}_{K,2}^{L(0)}(14, 15) = 2^{-1/2} [\overline{C}_{K,2}^{L(0)}(14) - \overline{C}_{K,-2}^{L(0)}(15)],$$

[where the superbars are defined by Eq. (A8) of I], and we have let $G_m(\Omega) \rightarrow \mathcal{D}_{K,M}^L(\Omega)$. The resulting equations for the general case (including anisotropic magnetic parameters and diffusion and orientation-dependent widths, W_e and W_n) are given in Bruno's thesis.³⁰

The numerical solution of the coupled equations for the coefficients can be accomplished by methods very similar to those used for unsaturated spectra (cf. I and II). The straightforward method is a back substitution technique, such as Gaussian elimination. Here, the most convenient procedure is to separate the coupled equations into their real and imaginary parts, as was done in II for a simple single line case, and then solve the resulting real equations.

The other method is to use a diagonalization

technique whereby a single diagonalization is needed to generate a spectrum. The two desirable characteristics required for this method to be effective are that (1) the matrix to be diagonalized have the sweep variable appearing only as a constant along the diagonal elements and (2) the matrix should be symmetric. Unfortunately, the separation of the equations into real and imaginary parts results in a set of equations which cannot be simply symmetrized. Instead, one may write down expressions for the $\bar{C}_{K,M}^{L(n)}(j)$ and their complex conjugates, while recognizing that the $\bar{b}_{K,0}^{L(0)}(j)$ (defined as the difference between $\bar{C}_{K,0}^{L(0)}(j)$ representing an eigenstate pair (cf. II) are real. One then achieves a symmetric matrix in terms of the coefficients $C_{K,M}^{L(1)}(j)$ and $iC_{KM}^{L(1)*}(j)$ for the three allowed and three average forbidden ESR transitions, also the $C_{K,M}^{L(0)}(j)$ and $-C_{K,M}^{L(0)}(j)$ for the three average NMR transitions of Eq. (A5), and finally the 3 $\bar{b}_{K,0}^{L(0)}(j)$.

Inspection of the resulting equations shows that the sweep variable ω_e only appears along the diagonal elements for the $n=1$ coefficients, and is totally absent from the $n=0$ terms. One may handle such cases by a simple partitioning technique. That is, the coupled equations obey the matrix equation

$$\mathbf{aC} = \mathbf{U} \tag{A6}$$

which we partition according to whether the diagonal term in \mathbf{a} contains ω_e , as

$$\begin{pmatrix} \mathbf{a}_{00} & \mathbf{a}_{01} \\ \mathbf{a}_{10} & \mathbf{a}_{11} \end{pmatrix} \begin{pmatrix} \mathbf{C}_0 \\ \mathbf{C}_1 \end{pmatrix} = \begin{pmatrix} \mathbf{0} \\ \mathbf{U}_1 \end{pmatrix} .$$

The subvector of coefficients \mathbf{C}_0 represents all the $n=0$ coefficients while \mathbf{C}_1 represents all the $n=1$ coefficients. Since \mathbf{a} is symmetric, one has \mathbf{a}_{00} and $\mathbf{a}_{10}^T = \mathbf{a}_{01}$. Since one is only interested in coefficients of the allowed transitions (cf. I and II) contained in \mathbf{a}_1 it is sufficient to solve the reduced matrix equation

$$\mathbf{a}'_{11}\mathbf{C}_1 = \mathbf{U}_1 \tag{A7}$$

where

$$\mathbf{a}'_{11} \equiv \mathbf{a}_{11} - \mathbf{a}_{10}(\mathbf{a}_{00})^{-1}\mathbf{a}_{01} . \tag{A8}$$

This partition method, in effect, adds terms which are proportional to d_e^2 to the matrix elements of the \mathbf{a}_{11} . Since these added matrix elements form a complex symmetric matrix themselves (because of the symmetry of \mathbf{a} itself) and they do not contain the sweep variable ω_e , the modified matrix \mathbf{a}'_{11} retains its symmetry and has ω_e as a constant along its diagonal. Thus \mathbf{a}'_{11} may be diagonalized with only one diagonalization per spectrum required. Also it is only necessary to first invert \mathbf{a}_{00} once. The computer program for simulating saturated

line shapes for an axial nitroxide is also listed in Bruno's thesis.³⁰ It allows for the \mathbf{a}'_{11} to be banded by truncating small terms involving d_e^2 that are outside an appropriate bandwidth.³²

We have studied the importance of saturation effects on the different coefficients $C_{K,M}^L(i)$ by examining the \mathbf{a}'_{11} matrix of Eq. (A8) obtained from typical computer simulations for $R \gg W_e$. We find that the saturation terms involving d_e^2 are very small for all matrix elements of \mathbf{a}'_{11} involving $C_{K,M}^L(i)$, where $L > 0$. This confirms our simpler discussion given in Sec. III.B. Thus only the $C_{0,0}^0(i)$ and $C_{0,0}^0(i)^*$ terms are significantly affected for $R \gg W_e$. In particular (1) the $C_{0,0}^0(i)$ terms for $i=1, 2$, and 3 are coupled strongly by terms in d_e^2 presumably due to coupled relaxation effects analogous to those seen in the motional narrowing region when $b \gtrsim 1$; (2) $C_{0,0}^0(i)$ and $C_{0,0}^0(i)^*$ are coupled strongly by terms in d_e^2 , and there is a large Im part of the diagonal contribution to $C_{0,0}^0(i)$, both of which are pure saturation effects. These observations suggest that much more compact computer programs for $R \gg W_e$ may be written by first (1) diagonalizing the unsaturated equations for all coefficients for $L \geq 2$ in the usual manner, and then (2) algebraically solving for the separate Real and Imaginary parts of the $C_{0,0}^0(i)$ [to which the appropriate saturation terms from Eq. (A8) have been added] in terms of their coupling to the coefficients for $L \geq 2$. This is analogous to an illustrative method given in Appendix A of II for a simpler case not involving saturation.

APPENDIX B: ORIENTATION-DEPENDENT SPIN-ROTATIONAL RELAXATION

One may develop simple orientation-dependent spin-rotational relaxation expressions based on Atkins's approximate analysis,³³ by assuming with him that (1) angular momentum relaxation and orientational relaxation are uncorrelated (but see Freed)³⁴ and (2) the angular momentum relaxation is naturally defined in the molecular frame. One then gets

$$W_e^{SR} = (kT/2\hbar^2) \{I_0[\tau_{J,0}/(1 + \omega_e^2\tau_{J,0}^2)]C_{xx}^2 \sin^2 \theta + I_1 \times [\tau_{J,1}/(1 + \omega_e^2\tau_{J,1}^2)]\{C_{xx}^2 + C_{yy}^2 - \frac{1}{2} \sin^2 \theta \times [C_{xx}^2 + C_{yy}^2] + (C_{xx}^2 - C_{yy}^2) \cos 2\varphi]\} \} \tag{B1a}$$

and

$$T_2^{-1}(\text{sec})^{SR} = (kT/\hbar^2) \{I_0\tau_{J,0}C_{xx}^2 \cos^2 \theta + I_1\tau_{J,1}(\sin^2 \theta/2) \times [C_{xx}^2 + C_{yy}^2 + (C_{xx}^2 - C_{yy}^2) \cos 2\varphi]\} . \tag{B1b}$$

Here I_0 and I_1 are the two principal moments of inertia (assuming axial symmetry) and $\tau_{J,0}$ and $\tau_{J,1}$ are the corresponding angular momentum relaxation times. Also θ is the angle between molecular and lab z axes, and φ is the azimuthal angle such that when $\alpha = 0$, the projection of the magnetic

field in the molecular x - y plane is along the molecular x axis. $T_2^{-1}(\text{sec})^{\text{SR}}$ represents only the secular contribution to the linewidth.

One may usually approximate the spin-rotation tensor components $C_{ii} \cong -\hbar(g_{ii} - g_e)/I_{ii}$. Thus for a nitroxide radical, since $g_{xx} - g_e \approx 0$, only the C_{xx} and C_{yy} terms in Eqs. (B1) should dominate. Then for $\theta = 0$, corresponding to the outer lines of the near rigid nitroxide spectrum:

$$W_e^{\text{SR}} \approx (kT/2\hbar^2) [I_1 \tau_{J,1} / (1 + \omega_e^2 \tau_{J,1}^2)] (C_{xx}^2 + C_{yy}^2), \quad (\text{B2a})$$

$$T_2^{-1}(\text{sec})^{\text{SR}} \approx 0, \quad (\text{B2b})$$

while for $\theta = \pi/2$ corresponding to the central region:

$$W_e^{\text{SR}} \approx (kT/4\hbar^2) [I_1 \tau_{J,1} / (1 + \omega_e^2 \tau_{J,1}^2)] [C_{xx}^2 + C_{yy}^2 - (C_{xx}^2 - C_{yy}^2) \cos 2\alpha] \quad (\text{B3a})$$

and

$$T_2^{-1}(\text{sec}) = (kT/2\hbar^2) I_1 \tau_{J,1} [(C_{xx}^2 + C_{yy}^2) + (C_{xx}^2 - C_{yy}^2) \times \cos 2\alpha] \quad (\text{B3b})$$

*Supported in part by a grant from the National Science Foundation (Grant No. GP-13780) and by the Materials Science Center, Cornell University.

¹Present address: Procter and Gamble Company, Miami Valley Laboratories, P. O. Box 39175, Cincinnati, OH 45239.

²Present address: Department of Chemistry, Stanford University, Palo Alto, CA 94305.

¹S. A. Goldman, G. V. Bruno, C. F. Polnaszek, and J. H. Freed, *J. Chem. Phys.* **56**, 716 (1972). This work will be referred to as I.

²J. H. Freed, G. V. Bruno, and C. F. Polnaszek, *J. Phys. Chem.* **75**, 3385 (1971). This work will be referred to as II.

³R. G. Kooser, W. V. Volland, and J. H. Freed, *J. Chem. Phys.* **50**, 5243 (1969).

⁴S. A. Goldman, G. V. Bruno, and J. H. Freed, *J. Phys. Chem.* **76**, 1858 (1972).

⁵R. C. McCalley, E. J. Schimshick, and H. M. McConnell, *Chem. Phys. Lett.* **13**, 115 (1972).

⁶J. S. Hyde, L. E. G. Eriksson, and A. Ehrenberg, *Biochim. Biophys. Acta* **222**, 688 (1970).

⁷J. S. Hyde and L. Dalton, *Chem. Phys. Lett.* **16**, 568 (1972).

⁸(a) J. H. Freed, *J. Chem. Phys.* **43**, 2312 (1965); (b) J. H. Freed, in *Electron-Spin Relaxation in Liquids*, edited by L. T. Muus and P. W. Atkins (Plenum, New York, 1972), Chap. XVIII.

⁹J. H. Freed, *J. Chem. Phys.* **41**, 2077 (1964).

¹⁰W. Moser and R. A. Howie, *J. Chem. Soc. A* **1968**, 3039.

¹¹J. H. Murib and D. M. Ritter, *J. Am. Chem. Soc.* **74**, 3394 (1952).

¹²(a) We are indebted to Z. Luz *et al.* for this gift. An earlier linewidth study on ¹⁷O-PADS was performed by Z. Luz, B. L. Silver, and C. Eden, *J. Chem. Phys.* **44**, 4421 (1966); (b) M. P. Eastman, G. V. Bruno, and J. H. Freed, *J. Chem. Phys.* **52**, 2511 (1970); (c) S. A. Goldman and J. H. Freed (unpublished).

¹³J. H. Freed and G. K. Fraenkel, *J. Chem. Phys.* **40**, 1815 (1964).

¹⁴M. T. Jones, *J. Chem. Phys.* **38**, 2892 (1963). Jones reports somewhat larger deviations from a Lorentzian (cf. Ref. 3 for a tabulation of his results). We note first of all that in this

work (as in I) 10 kHz field modulation was utilized, whereas Jones used 100 kHz, and the latter could affect the line shape. One computes (cf. Appendix to Ref. 3) an effective line broadening for $\delta = 155$ mG of 11 mG from 100 kHz modulation and only 0.11 mG from 10 kHz modulation. Also, while our field inhomogeneity is $\lesssim 5$ mG, Jones does not give his. Lastly, since such shape comparisons are performed relative to the measured derivative width, any instrumental effect on that width could significantly affect the results.

¹⁵M. T. Jones, M. Komarynsky, and R. D. Rataiczak, *J. Phys. Chem.* **75**, 2769 (1971).

¹⁶S. A. Goldman, Ph.D. thesis, Cornell University, Ithaca, NY, 1973.

¹⁷M. P. Eastman, R. G. Kooser, M. R. Das, and J. H. Freed, *J. Chem. Phys.* **51**, 2690 (1969).

¹⁸M. R. Das, S. B. Wagner, and J. H. Freed, *J. Chem. Phys.* **52**, 5404 (1970).

¹⁹Huntress [*Adv. Magn. Reson.* **4**, 1 (1970)] has criticized the linear combinations of symmetric rotor functions utilized in Ref. 9 for the asymmetric rotor functions as not consistent with standard conventions. However (when the instruction of footnote 20 of Ref. 9 is followed), one finds that the linear combinations given by Huntress are *identical* with those of Ref. 9.

²⁰If Eq. (4.3) for the nonsecular terms is used to calculate N for the frozen H₂O linewidth results given in I, a value of $N = 3 \pm 0.7$ is obtained in the region where nonsecular terms are important. This value is consistent with the $N = 2.9 \pm 0.3$ found for $\omega_0^2 \tau_R^2 \gg 1$.

²¹J. Hwang, R. Mason, and J. H. Freed (unpublished).

²²J. H. Freed and G. K. Fraenkel, *J. Chem. Phys.* **39**, 326 (1963).

²³J. H. Freed, see Ref. 8(b), Chap. VIII.

²⁴(a) B. J. Berne, J. P. Boone, and S. A. Rice, *J. Chem. Phys.* **45**, 1086 (1966); (b) K. S. Singwi and M. P. Tosi, *Phys. Rev.* **157**, 153 (1967); (c) P. C. Martin and S. Yip, *Phys. Rev.* **170**, 151 (1968).

²⁵R. Kubo, *Rep. Prog. Phys.* **29**, 255 (1966).

²⁶J. H. Freed, D. S. Leniart, and H. D. Connor, *J. Chem. Phys.* **58**, 3089 (1973).

²⁷The calculated contribution of anisotropic g -tensor relaxation to $W_e(0)$ is never more than a few percent of the total experimentally observed $W_e(0)$ over the entire motional narrowing region.

²⁸K. Krynicki and J. G. Powles, *J. Magn. Reson.* **6**, 539 (1972).

²⁹It does not appear possible to "explain" our observations with a Brown-Gutowsky-Shimomura-type jump model for spin-rotation [*J. Chem. Phys.* **38**, 76 (1963)] instead of Hubbard's Langevin model [*Phys. Rev.* **131**, 1155 (1963)]. We may write the former as replacing τ_J in Eq. (4.8b) by $\tau_J \approx (1/2)(\Delta^2/\tau)$, where τ is the mean time between jumps, which also appears in the Ivanov model for τ_R (cf. I). Also, Δ is the mean duration of a rotation and one assumes $\omega_e^2 \Delta^2 \gg 1$. We may then let $\Delta^2 \approx \langle \epsilon^2 \rangle_{\text{av}} / \langle \Omega^2 \rangle_{\text{av}} \approx (\langle \epsilon^2 \rangle_{\text{av}} / 3kT) I$, where $\langle \epsilon^2 \rangle_{\text{av}}$ is the mean-square jump angle for jump motion (cf. I), while Ω is an angular-velocity component and the second approximate equality follows from equipartition. Thus $\tau_J \approx (I/6kT) (\langle \epsilon^2 \rangle_{\text{av}} / \tau) = I/6kTB_2 \tau_R$, where B_2 is the model parameter of I which is determined by the nature of the jump model. [Equivalent expressions for τ_J have been given by O'Reilly, *J. Chem. Phys.* **56**, 2924 (1972) and by Hwang and Kivelson *J. Pure Appl. Chem.* (to be published)]. In particular, the simple jump-angle distribution function $W(\epsilon) \propto \sin[\frac{1}{2}\epsilon] e^{-\epsilon/\theta}$ (cf. I) leads to $B_2 = (1 + 6\theta^2)^{-1}$ for $\theta < \pi$. One might argue that $\theta^2 = \frac{1}{6} \langle \epsilon^2 \rangle_{\text{av}}$ gets larger with decreasing temperature, so that the behavior of τ_J is no longer simply dependent on τ_R^{-1} , but an anomalous temperature dependent behavior also should be observed

for $\tau_R^{-1} = 6B_2R = B_2\langle\epsilon^2\rangle_{av}/\tau$ if $\langle\epsilon^2\rangle_{av} < 1$, and this is not the case, cf. Figs. 9 and 10 of I. Also, it would be hard to justify an increase in τ_j with decreasing temperature needed for linewidth increase, as well as the much weaker nonsecular contribution.

³⁰G. V. Bruno, Ph.D. thesis, Cornell University, Ithaca, NY, 1973. (a) Actually, one may show from the general form of the solutions in terms of superpositions of "complex Lorentzians" (cf. Appendix A of II) that for the case of no saturation our use of an intrinsic T_2^{-1} gives results equivalent to those for inhomogeneous broadening with Lorentzian distribution. In the case of saturation, as is well known [cf. A. Abragam, *The Principles of Nuclear Magnetism* (Oxford U.P., New York, 1961), p. 51] the equivalence is not true even for a simple line. However, for a Lorentzian distribution for inhomogeneous broadening, the convolution with the homogeneous solution could be readily accomplished (again from the general form of the solutions) replacing ω everywhere by $\omega - iT_2^{-1}$ prior to taking the imaginary part of $\Sigma_{i=1}^3 C_{0,0}^i$ (i) as required in Eq. (A7) of I. This procedure is

not valid for the case of saturation when T_2^{-1} represents a homogeneous broadening.

³¹Note that an orientation-dependent secular $(T_2^{-1})^{SR}$ contribution would be contributing (from Appendix B) in the correct direction; in fact, for $C_{xx}^2 \approx C_{yy}^2$ and $\omega_e^2 \tau_{J,1}^2 \ll 1$, one has $(T_2^{-1})^{SR} = T_2^{-1}(\text{sec})^{SR} + W_e^{SR}$ in the ratio of $\frac{2}{3}$ for $\theta = 0$ and $\pi/2$, respectively. However, these terms will only make a negligible contribution to X in the slow-motional region.

³²There is a subtle problem which arises in the use of the Jacobi rotation method [R. G. Gordon and T. Messenger, cf. 8(b), Chap. XIII] for diagonalizing these matrices involving the complex conjugate coefficients. It arises for example, when one has $(A'_{11})_{ij} = \pm i(A'_{11})_{ik}$. Methods for dealing with this are discussed by Bruno.³⁰ In general, however, the truncation of small terms beyond an appropriate bandwidth effectively removes the difficulty.

³³P. W. Atkins, in *Electron-Spin Relaxation in Liquids*, edited by L. T. Muus and P. W. Atkins (Plenum, New York, 1972), Chap. XI.

³⁴J. H. Freed, *J. Chem. Phys.* **56**, 1407 (1972).